

RESEARCH

Open Access



# Comprehensive analysis revealed the immunoinflammatory targets of rheumatoid arthritis based on intestinal flora, miRNA, transcription factors, and RNA-binding proteins databases, GSEA and GSVA pathway observations, and immunoinfiltration typing

Yin Guan<sup>1</sup>, Yue Zhang<sup>1</sup>, Xiaoqian Zhao<sup>2</sup> and Yue Wang<sup>3\*</sup>

## Abstract

**Objective** Rheumatoid arthritis (RA) is a chronic inflammatory arthritis. This study aimed to identify potential biomarkers and possible pathogenesis of RA using various bioinformatics analysis tools.

**Methods** The GMrepo database provided a visual representation of the analysis of intestinal flora. We selected the GSE55235 and GSE55457 datasets from the Gene Expression Omnibus database to identify differentially expressed genes (DEGs) separately. With the intersection of these DEGs with the target genes associated with RA found in the GeneCards database, we obtained the DEGs targeted by RA (DERATGs). Subsequently, Disease Ontology, Gene Ontology, and the Kyoto Encyclopedia of Genes and Genomes were used to analyze DERATGs functionally. Gene Set Enrichment Analysis (GSEA) and Gene Set Variation Analysis (GSVA) were performed on the data from the gene expression matrix. Additionally, the protein-protein interaction network, transcription factor (TF)-targets, target-drug, microRNA (miRNA)-mRNA networks, and RNA-binding proteins (RBPs)-DERATGs correlation analyses were built. The CIBERSORT was used to evaluate the inflammatory immune state. The single-sample GSEA (ssGSEA) algorithm and differential analysis of DERATGs were used among the infiltration degree subtypes.

**Results** There were some correlations between the abundance of gut flora and the prevalence of RA. A total of 54 DERATGs were identified, mainly related to immune and inflammatory responses and immunodeficiency diseases. Through GSEA and GSVA analysis, we found pathway alterations related to metabolic regulations, autoimmune diseases, and immunodeficiency-related disorders. We obtained 20 hub genes and 2 subnetworks. Additionally, we found that 39 TFs, 174 drugs, 2310 miRNAs, and several RBPs were related to DERATGs. Mast, plasma, and naive B cells differed during immune infiltration. We discovered DERATGs' differences among subtypes using the ssGSEA algorithm and subtype grouping.

**Conclusions** The findings of this study could help with RA diagnosis, prognosis, and targeted molecular treatment.

\*Correspondence:

Yue Wang

wangyue@njucm.edu.cn

Full list of author information is available at the end of the article



© The Author(s) 2024. **Open Access** This article is licensed under a Creative Commons Attribution 4.0 International License, which permits use, sharing, adaptation, distribution and reproduction in any medium or format, as long as you give appropriate credit to the original author(s) and the source, provide a link to the Creative Commons licence, and indicate if changes were made. The images or other third party material in this article are included in the article's Creative Commons licence, unless indicated otherwise in a credit line to the material. If material is not included in the article's Creative Commons licence and your intended use is not permitted by statutory regulation or exceeds the permitted use, you will need to obtain permission directly from the copyright holder. To view a copy of this licence, visit <http://creativecommons.org/licenses/by/4.0/>. The Creative Commons Public Domain Dedication waiver (<http://creativecommons.org/publicdomain/zero/1.0/>) applies to the data made available in this article, unless otherwise stated in a credit line to the data.

**Keywords** Rheumatoid arthritis, Biomarkers, Pathogenesis, Bioinformatics analysis

## Introduction

A systemic autoimmune disease called rheumatoid arthritis (RA) is characterized by chronic inflammation that can damage joints and extra-articular organs [1]. It deteriorates intermittently, and without proper therapy, the symptoms worsen over time until the joints are irreparably damaged, leading to additional physical and psychological issues [2]. Therefore, managing and preventing RA requires early identification, diagnosis, and management. Some studies have shown that successful early intervention can significantly lower the financial burden of RA [3, 4]. However, the early onset of RA is typically misleading and challenging to identify at first [5]. Rheumatoid factors, anti-citrullinated protein antibodies (ACPAs), erythrocyte sedimentation rate, and C-reactive protein are the only four biomarkers currently used to identify RA, and each has some limitations [6]. Conventional, biological, and novel abiotic disease-modifying antirheumatic drugs are also recognized treatment options. A composite score is also used to quantify disease activity. While most patients respond to the available treatments and experience remission, many do not or are resistant [7]. Therefore, it is crucial to thoroughly comprehend the evolving mechanism of RA, search for novel signs that might be used for clinical diagnosis or identification of RA conditions, and design more efficient medication treatment targets. Based on the issues mentioned above and their significance, we suggest the following scientific questions: Several mechanisms can be identified and diagnosed in RA, and some genetic characteristics could serve as new targets for clinical treatment with current drugs.

We used various bioinformatics analytical methods to examine biomarkers and the inflammatory status of RA, including R packages from Bioconductor; the databases Gene Expression Omnibus (GEO), GMrepo, GeneCards, STRING, PharmGKB, DrugCentral, TargetScan, RNA-Binding Protein DataBase (RBPDB); the Cytoscape software; and the CIBERSORT website. This study provided a comprehensive reference for the current RA treatment conundrum by thoroughly explaining every aspect of the pathological molecular mechanism of RA and thoroughly analyzing the drugable targets that can be used for clinical diagnosis and treatment based on the mined key gene targets. Figure 1 depicts the workflow of the current study. Figure 2 summarizes the main findings of this study.

## Materials and methods

### The intestinal flora analysis

The GMrepo database (<https://gmrepo.humangut.info/home>) was used to retrieve relevant intestinal microbiotas of RA [8]. A correlation map was constructed between the relative abundance of gut microbiota and the prevalence of RA. A species co-occurrence network map was constructed by analyzing the relationships between species or genera of gut microbiota in patients with RA.

### Search strategy for GEO datasets

The following keywords were used to systematically retrieve 127 datasets from the GEO database (<https://www.ncbi.nlm.nih.gov/geo/>) (((rheumatoid arthritis[MeSH Terms]) OR rheumatoid arthritis) AND human[Organism]) AND Expression profiling by array[Filter]) AND (“2012/01/01”[Publication Date]: “2022/01/01”[Publication Date]). Exclusion criteria: (1) Excluded those with a small sample size (sample size < 20), (2) Excluded those with irrelevant datasets (no rheumatoid arthritis), (3) Excluded blood samples and/or cell samples, (4) Excluded those with significant interference from the drug, vaccine, age, environmental, psychological, regional genetic, or epidemiological factors, (5) Lack of normal samples, and (6) Excluded those with unbalanced sample sizes (listed in Fig. 1).

### Data download and preprocessing

The GEO database (<https://www.ncbi.nlm.nih.gov/geo/>) was used to download microarray datasets GSE55235 [9] and GSE55457 [9] using the R package (GEOquery) [10]. Additionally, all dataset samples were generated from *Homo sapiens* using the GPL96 [HG-U133A] Affymetrix Human Genome U133A Array platform. The GSE55235 dataset contained 10 samples from patients with RA and 10 samples from healthy volunteers. In contrast, the GSE55457 dataset contained 13 samples from patients with RA and 10 samples from healthy volunteers, which were used in this study. RMA algorithm from the Affy package in R was used to normalize the data [11]. With the RNASeqSampleSize package, statistical power analysis of the data is done [12].

### Differentially Expressed Genes (DEGs) screening and functional analysis

The DEGs for the two datasets, GSE55235 and GSE55457, were identified using limma [13]. The DEGs were then displayed using the R program as Volcano plots and

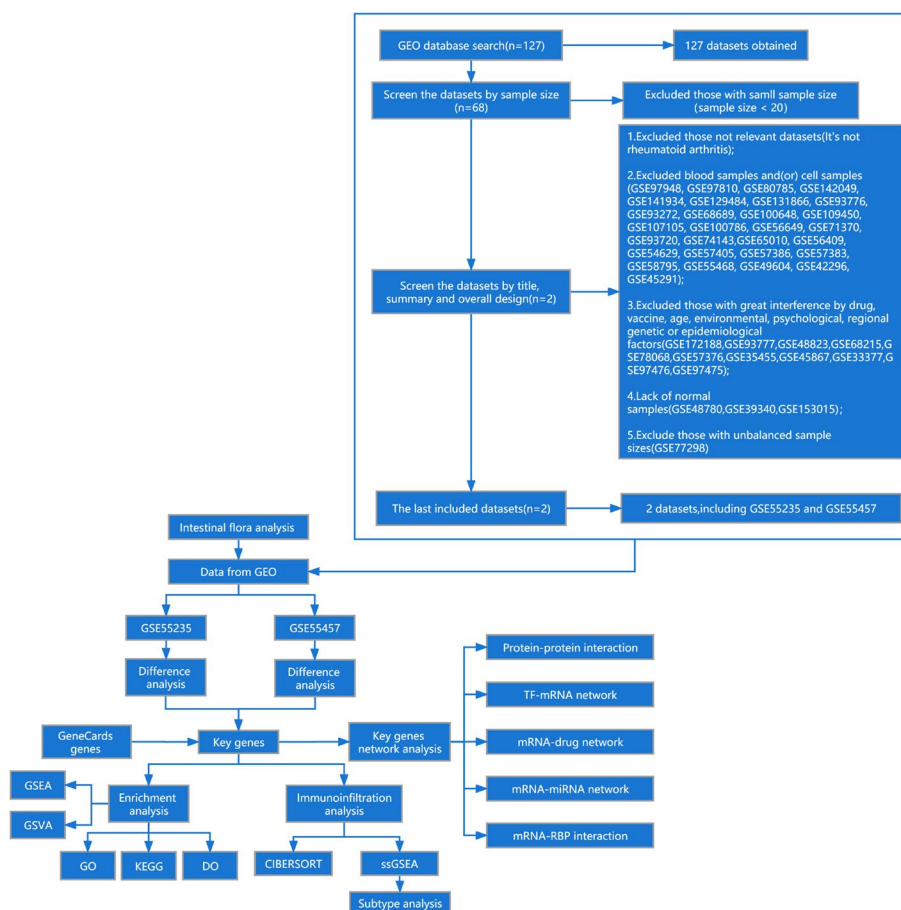


**Fig. 1** Flowchart of the analytical process

Heat maps using the ggplot2 and pheatmap packages, respectively.  $|\log_2$  of the Fold Change ( $\log_2FC$ ) $>1$  and adjusted  $P$ -value $<0.05$  were used to recruit DEGs. The GeneCards database (<http://www.genecards.org/>) was used to find the RA target genes (RATGs) [14] by searching the keyword “rheumatoid arthritis.” Next, the DEGs targeted by RA (DERATGs) were filtered by overlapping the DEGs and RATGs using a Venn diagram. Subsequently, the clusterProfiler package [15] was used to handle Gene Ontology (GO) function, and Kyoto Encyclopedia of Genes and Genomes (KEGG) pathway enrichments on DERATGs and Disease Ontology (DO) enrichments were performed for DERATGs using the DOSE package [16]. Adjusted  $P$ -value $<0.05$  was considered statistically different. Meanwhile, the Gene Set Enrichment Analysis (GSEA) was performed on all RA genes (previously ranked based on their  $\log_2FC$  between analyzed groups) using the clusterProfiler package. It was thought that the enrichment was significant if the nominal false discovery rate (FDR) $<0.25$  and  $P$ -value $<0.05$  by referencing the “c2.cp.kegg.v7.5.1.symbols.gmt” gene set.

Utilizing the gene set variation analysis (GSVA) package [17], RA gene expression matrix data were subjected to GSVA. The differential pathways were filtered according to adjusted  $P$ -value $<0.05$  and  $|\log_2FC|>0.263$ .

### Construction of the Protein–Protein Interaction (PPI) network

The PPI network of the DERATGs was analyzed using the interaction relation in the database STRING (<https://string-db.org/>) [18]. Network node attributes were calculated using NetworkAnalyzer in Cytoscape [19]. Cytoscape’s cytoHubba plugin [20] predicted important nodes (or hub proteins). The subnetworks were extracted from the whole PPI network using the MCODE [20].

### Construction of DERATGs related networks

Transcription factor (TF)-target relationships data was obtained from the TRRUST database (<https://www.grnpedia.org/trrust/>) [21]. Meanwhile, the Cytoscape software also showed its relational network. The database PharmGKB (<https://www.pharmgkb.org/>) [22] and

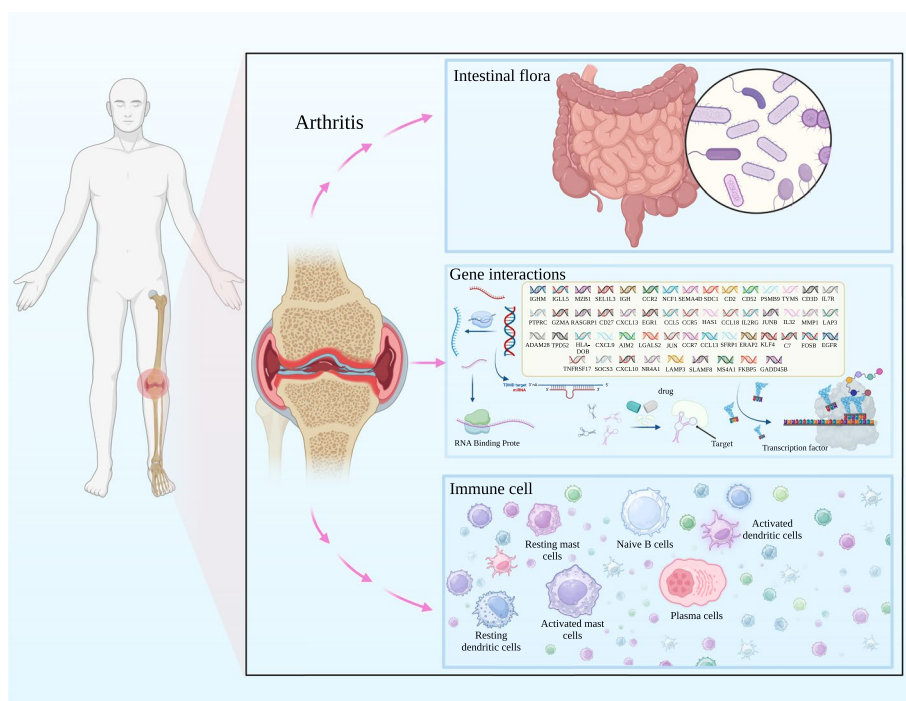


**Fig. 2** Main discovery mechanism diagram

the database DrugCentral (<https://drugcentral.org/>) [23] forecasted the association of interactions between DERATGs and medicinal compounds. The microRNA (miRNA)-mRNA regulatory networks were constructed using the TargetScan database ([http://www.targetscan.org/vert\\_71/](http://www.targetscan.org/vert_71/)) [24] to predict the potentially related miRNA of DERATGs. The database RBPDB (<http://rbpdb.ccb.utoronto.ca/>) was used to predict the RNA-binding proteins of DERATGs [25].

#### Analysis of immune cell infiltration

CIBERSORT deconvolves the transcriptome expression matrix to determine the make-up and number of immune cells within a mixed cell population using linear support vector regression [26]. We entered the gene expression matrix data into CIBERSORT, filtered samples with a  $P$ -value  $< 0.05$ , and created the immune cell infiltration matrix. The ggheatmap package generated heat maps depicting the 22 immune cells during each sample. Box-plots were created using the ggplot2 and ggpubr packages to investigate differences in immune infiltrating cells between groups, with  $P < 0.05$  as the screening standard.

#### Subgroup evaluation

Twenty-eight RA samples were given enrichment scores using single-sample GSEA (ssGSEA) [27]. Following that, depending on immune infiltrating cell expression, we categorized RA into two subtypes (Cluster1 and Cluster2).

We investigated the DEGs of DERATGs between these subtypes in the GSE55235 and the GSE55457 datasets.

## Results

### Statistical analyses of the intestinal microbiota

A correlation map between the abundance of gut microbiota and the prevalence of RA was created using the GMrepo database (Fig. 3A). The percentage of samples that contained species/genera  $> 0.01\%$  abundance threshold was counted, and the mean/median relative abundance of species in all RA samples was also summarized. The species co-occurrence network diagram (Fig. 3B) was constructed, with nodes representing species or genera co-occurring with other species or genera in this RA sample. The number of connected network nodes affects the size, and the width of the lines (Pearson's correlation) represents relationships between species or genera characterized by co-occurrence.

### Data selection and DERATGs screening

According to the GEO data platform, the analysis data were summarized and sorted (Table 1). Following data comparison, it was determined that the sample sizes for the RA and the normal groups were roughly balanced, and an examination of the statistical power of the sample sizes of the ss data sets was conducted (Table 1), laying the groundwork for further analysis. The GSE55235 dataset's gene expression matrix was initially standardized and



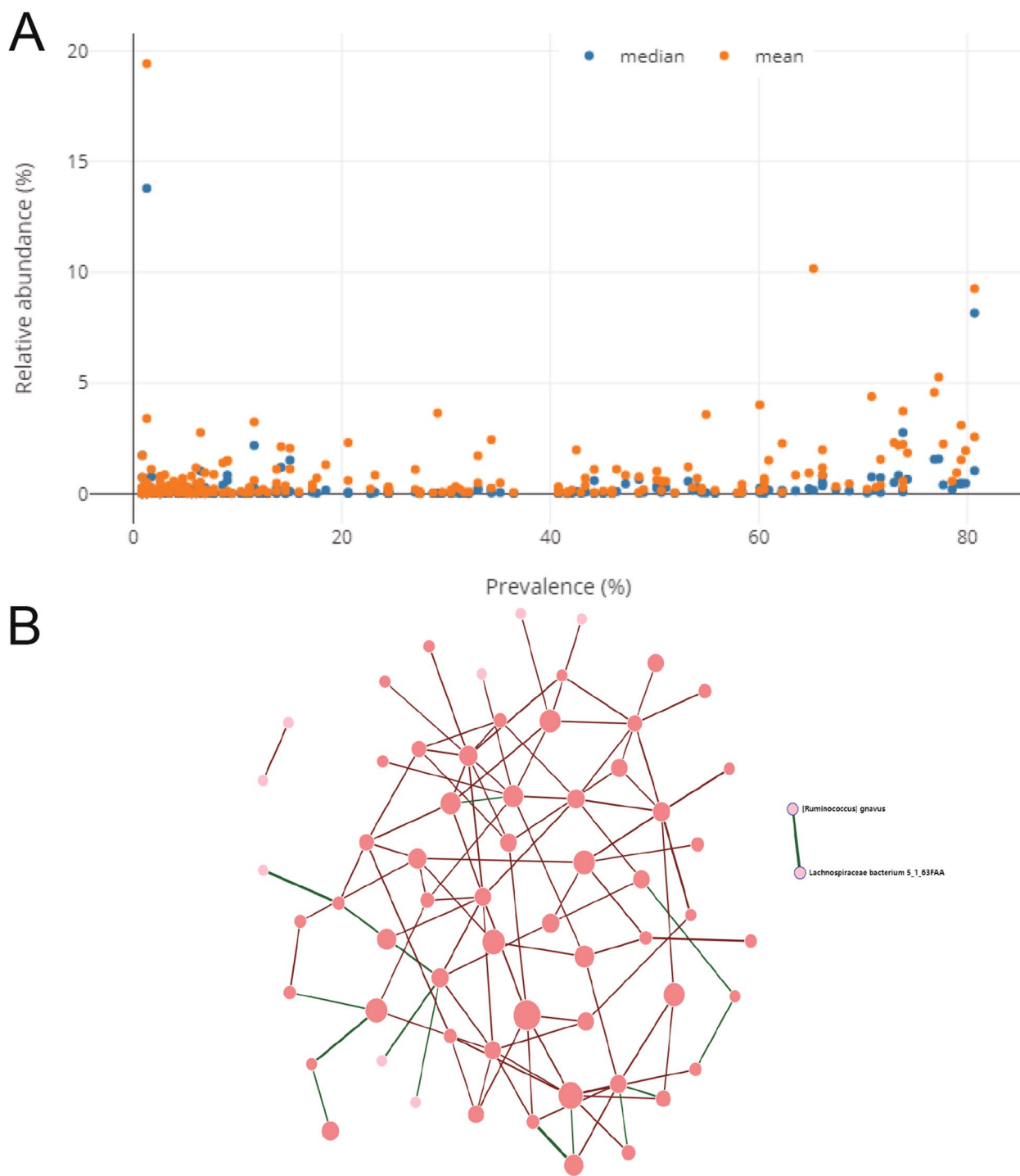


**Fig. 3** Data on intestinal microbiota in rheumatoid arthritis. **A** Prevalence abundance map analysis. **B** Species co-occurrence network diagram. Green indicates positive, and red indicates negative correlations

processed. As shown in the Volcano plot (Fig. 4A) created using R software after data preprocessing, the gene expression matrix yielded 296 upregulated and 248 downregulated genes. The top 10 genes with the most significant

differences were identified. Subsequently, we also showed the heat map of DEGs for the GSE55235 dataset (Fig. 4B). Following standardization, the GSE55457 dataset was compared to the normal samples. Differential analysis was

**Table 1** Data information summary

GEO accession	Platforms	Sample		Statistical Power
GSE55235	GPL96	Normal	10	0.8466
		RA	10	
GSE55457	GPL96	Normal	10	0.9212
		RA	13	

conducted to obtain 114 genes that were upregulated and 51 genes that were downregulated. The Volcanic plot was shown (Fig. 4C). Meanwhile, the heat map was also used to show the expression between samples (Fig. 4D). GeneCards retrieved the disease targets of RA (Supplement Spreadsheet S1). Differential genes of the two datasets and the target genes of the GeneCards database intersected, and 54 DERATGs were finally screened out (Fig. 4E).

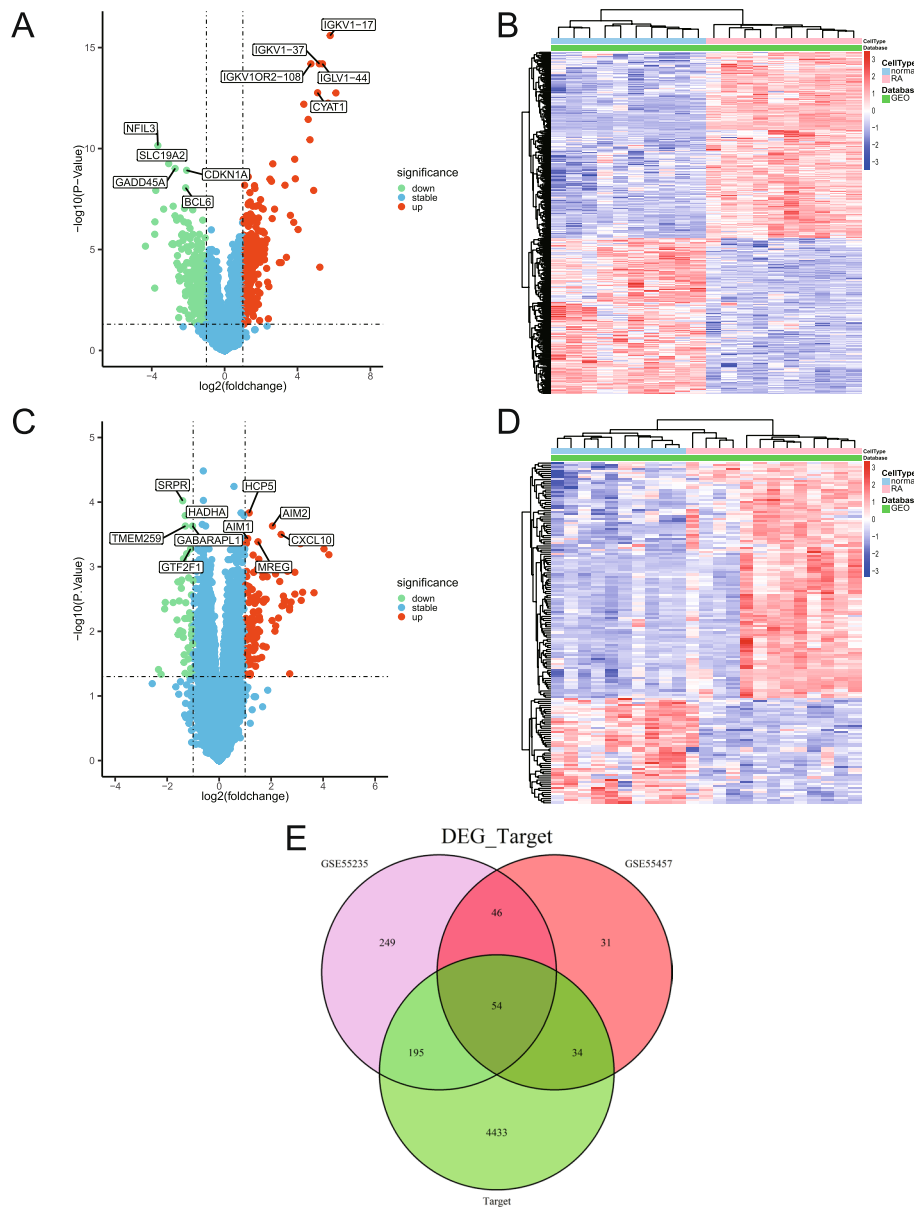


**Fig. 4** Differentially expressed genes targeted by RA (DERATGs) screening. **A** Volcano plot of GSE55235. Red signifies upregulated DEGs, green signifies downregulated DEGs, and blue signifies no DEGs. **B** Heat map of GSE55235. Blue represents the normal group, and red represents the rheumatoid arthritis (RA) group. **C** Volcano plot of GSE55457. Red indicates upregulated DEGs, green indicates downregulated DEGs, and blue indicates no DEGs. **D** Heat map of GSE55457. Blue represents the normal group, and red represents the RA group. **E** Comprehensive screening of DERATGs by DEGs of the two datasets and GeneCards

### GO, KEGG, and DO enrichment analysis

Then, functional enrichment analyses for GO (Table 2), KEGG (Table 3), and DO (Table 4) were carried out on DERATGs. The GO results confirmed that DERATGs were primarily linked to the cytokine-mediated signaling pathway, clathrin-coated endocytic vesicle membrane, G protein-coupled receptor binding, and other biological phenomena (Fig. 5A-C). The KEGG results showed that the tumor necrosis factor signaling pathway, chemokine signaling pathway, osteoclast differentiation, and other pathways had higher DERATG concentrations than other pathways (Fig. 5D-F). According to DO findings, DERATGs were particularly enriched in myeloma, bone marrow cancer, multiple myeloma, and other diseases (Fig. 5G-I).

### GSEA and GSVA analysis

Our reference gene set was “c2.cp.kegg.v7.5.1.symbols.gmt.” The two datasets were subjected to a GSEA enrichment analysis to identify significant enrichment according to the FDR criteria  $< 0.25$  and  $P < 0.05$ . (Table 5). The GSEA enrichment analysis revealed that the DERATGs in the GSE55235 dataset exist and are also significantly enriched in the upregulated pathways, such as an intestinal immune network for immunoglobulin (Ig)A production, allograft rejection,

**Table 3** KEGG enrichment summary

ID	Description	<i>p.adjust</i>	<i>qvalue</i>	Count
hsa04061	Viral protein interaction with cytokine and cytokine receptor	<0.001	<0.001	10
hsa04060	Cytokine-cytokine receptor interaction	<0.001	<0.001	14
hsa04062	Chemokine signaling pathway	<0.001	<0.001	10
hsa05340	Primary immunodeficiency	0.001	0.001	4
hsa04640	Hematopoietic cell lineage	0.004	0.003	5
hsa04668	TNF signaling pathway	0.006	0.005	5
hsa04380	Osteoclast differentiation	0.01	0.008	5

autoimmune thyroid disease, etc. (Fig. 6A), and are also significantly enriched in the downregulated pathways, such as ribosome biogenesis in eukaryotes, basal cell carcinoma, mitophagy-animal, and so on (Fig. 6B). Similarly, the GSEA enrichment analysis on the GSE55457 dataset (Fig. 6D, E) revealed very high similarity with the GSE55235 dataset, demonstrating the efficacy of DERATGs and enabling further analysis. GSVA enrichment analysis was performed on the GSE55235 and the GSE55457 datasets, and distinct pathways were displayed (Table 6). The differential

**Table 2** GO enrichment summary

Ontology	ID	Description	<i>p.adjust</i>	Count
BP	GO:0019221	cytokine-mediated signaling pathway	<0.001	15
BP	GO:0070098	chemokine-mediated signaling pathway	<0.001	9
BP	GO:1990868	response to chemokine	<0.001	9
BP	GO:1990869	cellular response to chemokine	<0.001	9
BP	GO:1903131	mononuclear cell differentiation	<0.001	14
BP	GO:0030098	lymphocyte differentiation	<0.001	13
BP	GO:0030595	leukocyte chemotaxis	<0.001	10
BP	GO:0060326	cell chemotaxis	<0.001	11
BP	GO:0006959	humoral immune response	<0.001	11
BP	GO:0042113	B cell activation	<0.001	11
CC	GO:0009897	external side of plasma membrane	<0.001	15
CC	GO:0030669	clathrin-coated endocytic vesicle membrane	0.043	3
MF	GO:0042379	chemokine receptor binding	<0.001	7
MF	GO:0008009	chemokine activity	<0.001	6
MF	GO:0048020	CCR chemokine receptor binding	<0.001	5
MF	GO:0001664	G protein-coupled receptor binding	<0.001	8
MF	GO:0140375	immune receptor activity	<0.001	6
MF	GO:0005125	cytokine activity	<0.001	7
MF	GO:0004896	cytokine receptor activity	<0.001	5
MF	GO:0005126	cytokine receptor binding	<0.001	7
MF	GO:0045236	CXCR chemokine receptor binding	<0.001	3
MF	GO:0016493	C–C chemokine receptor activity	<0.001	3

**Table 4** DO enrichment summary

ID	Description	p.adjust	qvalue	Count
DOID:0070004	myeloma	< 0.001	< 0.001	14
DOID:4960	bone marrow cancer	< 0.001	< 0.001	14
DOID:9538	multiple myeloma	< 0.001	< 0.001	12
DOID:526	Human immunodeficiency virus infectious disease	< 0.001	< 0.001	10
DOID:0050338	primary bacterial infectious disease	< 0.001	< 0.001	11
DOID:2237	hepatitis	< 0.001	< 0.001	14
DOID:104	bacterial infectious disease	< 0.001	< 0.001	11
DOID:1036	chronic leukemia	< 0.001	< 0.001	10
DOID:2789	parasitic protozoa infectious disease	< 0.001	< 0.001	8
DOID:612	primary immunodeficiency disease	< 0.001	< 0.001	9

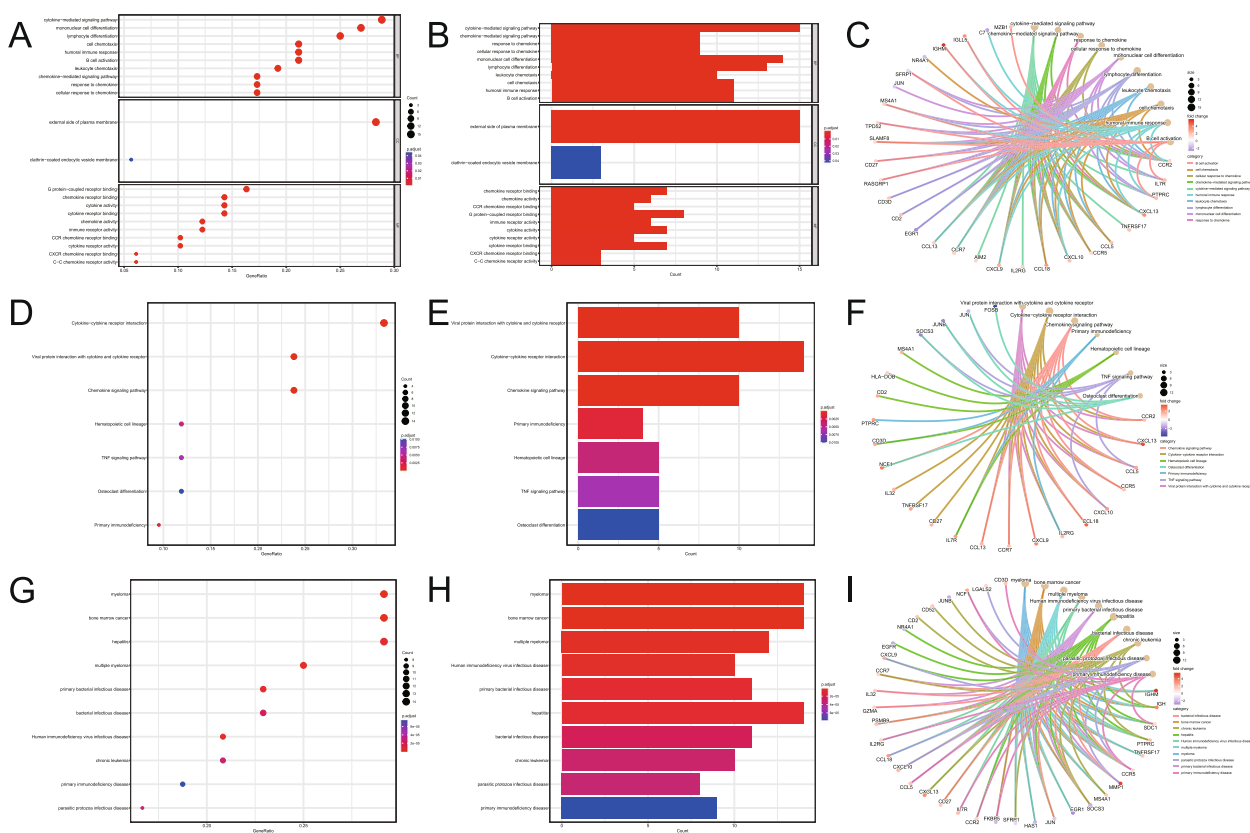


**Fig. 5** Differentially expressed genes targeted by RA (DERATGs) functional correlation evaluation. **A** DERATGs' Gene Ontology (GO) biological function enrichment evaluation. The X-axis represents the enrichment of DERATG in GO entries, and the color of the dots represents the adjusted *P*-value: redder is displayed when the adjusted *P*-value is lower, and bluer is displayed when the adjusted *P*-value is higher. The size of the dots serves as a proxy for the number of enriched genes. **B, C** Exhibition of DERATGs GO biological function enrichment. **D** DERATGs' KEGG pathway enrichment study. The size of the dots indicates the number of enriched genes. **E, F** DERATGs KEGG biological function enrichment exhibition. **G** DERATGs' enrichment study using Disease Ontology (DO). The x-axis represents the percentage of DERATGs enriched in the disease team, the y-axis displays the names of the enrichment diseases, and the dot color indicates the adjusted *P*-value: a lower adjusted *P*-value corresponds to red color, and a higher adjusted *P*-value corresponds to blue color. The size of the dots serves as a proxy for the number of enriched genes. **H, I** DERATGs DO enrichment exhibition

**Table 5** GSEA enrichment summary

GEO accession	ID	Description	enrichmentScore	pvalue	qvalues
GSE55235	hsa05310	Asthma	0.876	< 0.001	< 0.001
	hsa05330	Allograft rejection	0.842	< 0.001	< 0.001
	hsa05340	Primary immunodeficiency	0.841	< 0.001	< 0.001
	hsa05320	Autoimmune thyroid disease	0.837	< 0.001	< 0.001
	hsa04672	Intestinal immune network for IgA production	0.826	< 0.001	< 0.001
	hsa05150	Staphylococcus aureus infection	0.793	< 0.001	< 0.001
	hsa04940	Type I diabetes mellitus	0.773	< 0.001	< 0.001
	hsa05332	Graft-versus-host disease	0.773	< 0.001	< 0.001
	hsa04612	Antigen processing and presentation	0.739	< 0.001	< 0.001
	hsa05322	Systemic lupus erythematosus	0.736	< 0.001	< 0.001
	hsa03008	Ribosome biogenesis in eukaryotes	-0.591	0.004	0.017
	hsa05217	Basal cell carcinoma	-0.606	0.002	0.01
	hsa04137	Mitophagy—animal	-0.607	< 0.001	0.006
	hsa04978	Mineral absorption	-0.617	0.003	0.013
	hsa00830	Retinol metabolism	-0.635	0.004	0.015
	hsa05213	Endometrial cancer	-0.64	< 0.001	0.003
	hsa03040	Spliceosome	-0.649	< 0.001	< 0.001
	hsa04710	Circadian rhythm	-0.685	0.006	0.022
	hsa05216	Thyroid cancer	-0.693	< 0.001	0.006
	GSE55457	hsa00350	Tyrosine metabolism	-0.769	< 0.001
hsa05340		Primary immunodeficiency	0.785	< 0.001	< 0.001
hsa05330		Allograft rejection	0.724	< 0.001	< 0.001
hsa05320		Autoimmune thyroid disease	0.683	< 0.001	< 0.001
hsa04940		Type I diabetes mellitus	0.672	< 0.001	< 0.001
hsa05332		Graft-versus-host disease	0.661	< 0.001	0.002
hsa04672		Intestinal immune network for IgA production	0.657	< 0.001	< 0.001
hsa04061		Viral protein interaction with cytokine and cytokine receptor	0.643	< 0.001	< 0.001
hsa04062		Chemokine signaling pathway	0.566	< 0.001	< 0.001
hsa04612		Antigen processing and presentation	0.563	< 0.001	0.001
hsa04650		Natural killer cell mediated cytotoxicity	0.562	< 0.001	< 0.001
hsa05412		Arrhythmogenic right ventricular cardiomyopathy	-0.432	0.007	0.034
hsa04928		Parathyroid hormone synthesis, secretion and action	-0.444	< 0.001	0.006
hsa05410		Hypertrophic cardiomyopathy	-0.455	0.001	0.008
hsa04520		Adherens junction	-0.477	0.001	0.01
hsa05031		Amphetamine addiction	-0.479	0.004	0.023
hsa04923		Regulation of lipolysis in adipocytes	-0.481	0.004	0.024
hsa05210		Colorectal cancer	-0.488	< 0.001	0.002
hsa04350		TGF-beta signaling pathway	-0.506	< 0.001	0.001
hsa04979		Cholesterol metabolism	-0.541	< 0.001	0.006
hsa04977	Vitamin digestion and absorption	-0.666	0.005	0.028	

pathways in the GSE55235 dataset included autoimmune thyroid disease, the intestinal immune network for IgA production, viral myocarditis, and so on (Fig. 6C). Its outcomes matched those of the GSE55457's GSVA differential pathway (Fig. 6F).

#### Analysis of PPI using DERATGs

PPI of 54 DERATGs was assessed using the database STRING, and 47 DERATGs were discovered to have a PPI link, which was as follows: *C7, ERAP2, LAP3, RAS-GRP1, SEMA4D, SFRP1, TYMS, LAMP3, NCF1, AIM2,*



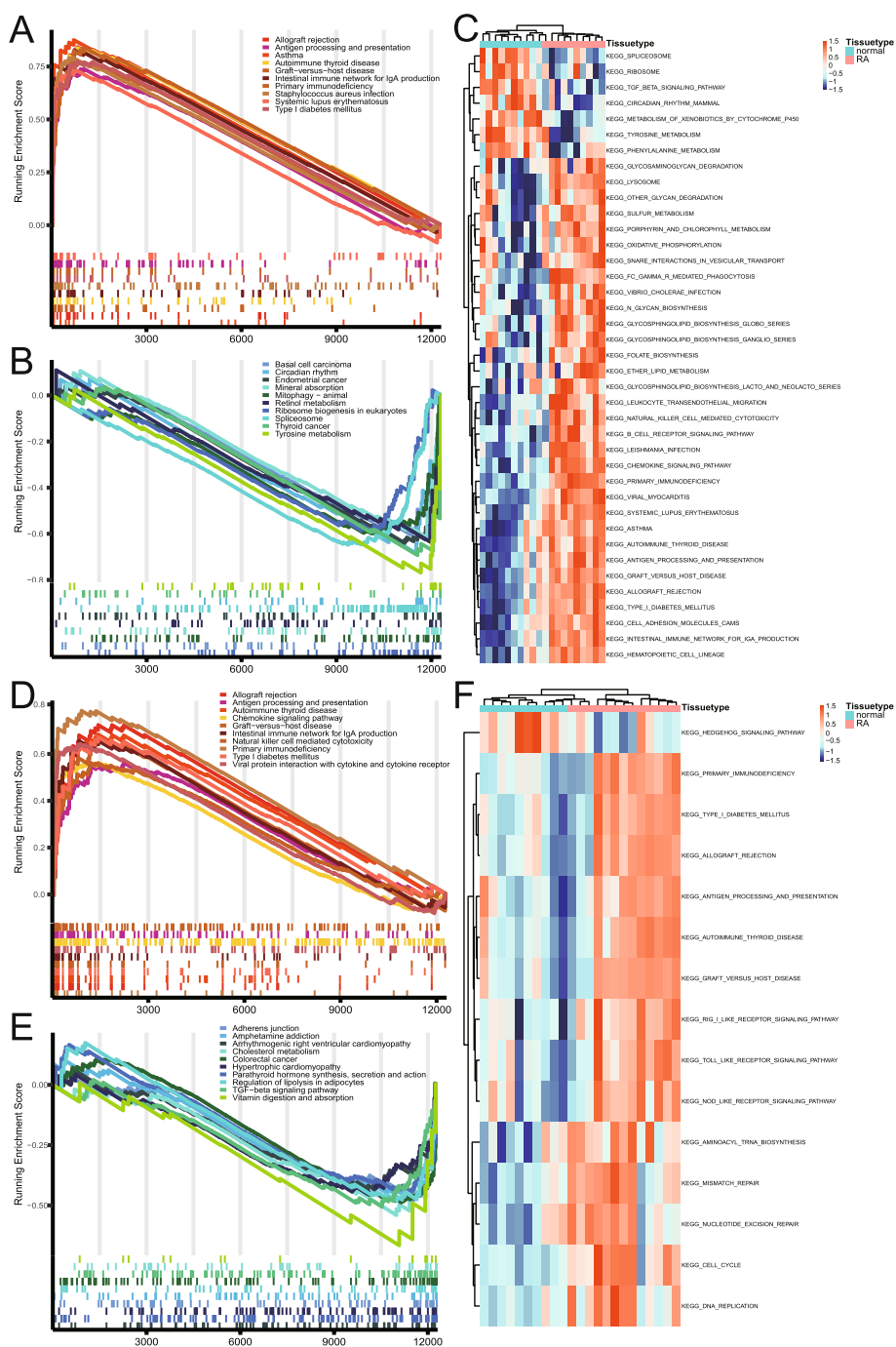


**Fig. 6** Gene Set Enrichment Analysis and Gene Set Variation Analysis of the GSE55235 and GSE55457 datasets. **A** Analysis of differential genes' upregulated pathways in the GSE55235 dataset. **B** Analysis of differential genes' downregulated pathways in the GSE55235 dataset. **C** Differentially enriched pathways in the GSE55235 dataset. **D** Analysis of differential genes' upregulated pathways in the GSE55457 dataset. **E** Analysis of differential genes' downregulated pathways in the GSE55457 dataset. **F** Differentially enriched pathways in the GSE55457 dataset

*HLA-DOB, IL32, MZB1, PSMB9, SLAMF8, TNFRSF17, GADD45B, FOSB, JUNB, KLF4, MMP1, EGRI, CCL13, SOCS3, IGLL5, NR4A1, CCL18, IGHV4-38-2, CD52, MS4A1, CD3D, EGFR, IL2RG, SDC1, GZMA,*

*CCR2, CXCL13, CXCL9, CCR5, IL7R, JUN, CCR7, CD2, CXCL10, CD27, CCL5, and PTPRC.* The number of interactions for each DERATG was visualized (Fig. 7A). Additionally, Cytoscape was used to display

**Table 6** GSVA enrichment summary

GEO accession	Description	logFC	AveExpr	P.Value	adj.P.Val
GSE55235	KEGG_PRIMARY_IMMUNODEFICIENCY	0.723	0.004	<0.001	<0.001
	KEGG_ALLOGRAFT_REJECTION	0.702	0.016	<0.001	<0.001
	KEGG_VIRAL_MYOCARDITIS	0.492	0.011	<0.001	<0.001
	KEGG_SYSTEMIC_LUPUS_ERYTHEMATOSUS	0.469	0.007	<0.001	<0.001
	KEGG_LEISHMANIA_INFECTION	0.479	-0.001	<0.001	<0.001
	KEGG_INTESTINAL_IMMUNE_NETWORK_FOR_IGA_PRODUCTION	0.564	0.008	<0.001	<0.001
	KEGG_ANTIGEN_PROCESSING_AND_PRESENTATION	0.508	-0.004	<0.001	<0.001
	KEGG_GRAFT_VERSUS_HOST_DISEASE	0.633	0.03	<0.001	<0.001
	KEGG_TYPE_I_DIABETES_MELLITUS	0.528	0.014	<0.001	<0.001
	KEGG_ASTHMA	0.549	0.032	<0.001	<0.001
	KEGG_CELL_ADHESION_MOLECULES_CAMS	0.436	0.021	<0.001	<0.001
	KEGG_LYSOSOME	0.488	0.029	<0.001	<0.001
	KEGG_CHEMOKINE_SIGNALING_PATHWAY	0.322	0.014	<0.001	<0.001
	KEGG_LEUKOCYTE_TRANSENDOTHELIAL_MIGRATION	0.352	0.003	<0.001	<0.001
	KEGG_AUTOIMMUNE_THYROID_DISEASE	0.512	0.007	<0.001	<0.001
	KEGG_FC_GAMMA_R_MEDIATED_PHAGOCYTOSIS	0.345	0.009	<0.001	<0.001
	KEGG_HEMATOPOIETIC_CELL_LINEAGE	0.318	0.012	<0.001	<0.001
	KEGG_B_CELL_RECEPTOR_SIGNALING_PATHWAY	0.328	0.008	<0.001	0.001
	KEGG_GLYCOSPHINGOLIPID_BIOSYNTHESIS_GLOBO_SERIES	0.419	0.004	<0.001	0.001
	KEGG_NATURAL_KILLER_CELL_MEDIATED_CYTOTOXICITY	0.346	0.003	<0.001	0.001
	KEGG_N_GLYCAN_BIOSYNTHESIS	0.384	0.012	<0.001	0.002
	KEGG_PORPHYRIN_AND_CHLOROPHYLL_METABOLISM	0.343	0.028	<0.001	0.002
	KEGG_FOLATE_BIOSYNTHESIS	0.418	0.006	<0.001	0.003
	KEGG_VIBRIO_CHOLERAЕ_INFECTION	0.343	0.006	<0.001	0.004
	KEGG_GLYCOSPHINGOLIPID_BIOSYNTHESIS_GANGLIO_SERIES	0.443	0.017	<0.001	0.004
	KEGG_SULFUR_METABOLISM	0.461	0.027	<0.001	0.005
	KEGG_OTHER_GLYCAN_DEGRADATION	0.45	0.022	0.003	0.017
	KEGG_SNARE_INTERACTIONS_IN_VESICULAR_TRANSPORT	0.29	0.014	0.003	0.017
	KEGG_ETHER_LIPID_METABOLISM	0.276	-0.009	0.004	0.02
	KEGG_GLYCOSAMINOGLYCAN_DEGRADATION	0.307	0.018	0.004	0.02
	KEGG_OXIDATIVE_PHOSPHORYLATION	0.338	-0.003	0.006	0.027
	KEGG_GLYCOSPHINGOLIPID_BIOSYNTHESIS_LACTO_AND_NEOLACTO_SERIES	0.272	0	0.007	0.03
	KEGG_TGF_BETA_SIGNALING_PATHWAY	-0.352	-0.012	<0.001	<0.001
	KEGG_SPLICEOSOME	-0.43	-0.035	<0.001	0.001
	KEGG_METABOLISM_OF_XENOBIOTICS_BY_CYTOCHROME_P450	-0.281	-0.015	<0.001	0.002
	KEGG_CIRCADIAN_RHYTHM_MAMMAL	-0.487	-0.043	<0.001	0.003
	KEGG_TYROSINE_METABOLISM	-0.264	0.001	<0.001	0.005
	KEGG_RIBOSOME	-0.365	-0.031	0.008	0.03
	KEGG_PHENYLALANINE_METABOLISM	-0.278	0.009	0.009	0.033

**Table 6** (continued)

GEO accession	Description	logFC	AveExpr	P.Value	adj.P.Val
GSE55457	KEGG_MISMATCH_REPAIR	0.477	0.006	<0.001	0.005
	KEGG_CELL_CYCLE	0.325	0.003	<0.001	0.005
	KEGG_DNA_REPLICATION	0.456	-0.011	<0.001	0.015
	KEGG_RIG_I_LIKE_RECEPTOR_SIGNALING_PATHWAY	0.274	0.023	<0.001	0.015
	KEGG_TYPE_I_DIABETES_MELLITUS	0.459	0.011	<0.001	0.015
	KEGG_AMINOACYL_TRNA_BIOSYNTHESIS	0.367	0.011	<0.001	0.015
	KEGG_AUTOIMMUNE_THYROID_DISEASE	0.427	0.01	<0.001	0.015
	KEGG_GRAFT_VERSUS_HOST_DISEASE	0.505	0.025	<0.001	0.015
	KEGG_ALLOGRAFT_REJECTION	0.533	0.018	<0.001	0.015
	KEGG_PRIMARY_IMMUNODEFICIENCY	0.492	0.002	<0.001	0.016
	KEGG_TOLL_LIKE_RECEPTOR_SIGNALING_PATHWAY	0.267	0.024	0.002	0.025
	KEGG_NUCLEOTIDE_EXCISION_REPAIR	0.295	0.006	0.002	0.025
	KEGG_ANTIGEN_PROCESSING_AND_PRESENTATION	0.344	0.017	0.003	0.027
	KEGG_NOD_LIKE_RECEPTOR_SIGNALING_PATHWAY	0.311	0.012	0.003	0.027
	KEGG_HEDGEHOG_SIGNALING_PATHWAY	-0.274	-0.014	0.001	0.021

the network (Fig. 7B). The node degree increases with an increase in DERATGs size. In contrast, the number of edge interfaces increases as line thickness increases. The cytoHubba tool was used to search hub nodes in the network, and MCC was used to determine the top 20 genes as key gene nodes. The score increases as the node color becomes darker (Fig. 7C). The subnetwork is built using the MCODE, which is used to cluster and build functional modules in the network (Fig. 7D, E), and the construction of the subnetwork reveals the dense areas of potential biological functions.

#### Construction of TF-targets, miRNA-mRNA network, and RBP-DERATGs correlation analysis

The TRRUST database predicted the TFs of 54 DERATGs. Thirty-nine TFs were obtained, corresponding to 25 DERATGs. The network visualized the regulatory relationships (Fig. 8A). The TargetScan database also predicted the miRNAs of DERATGs, and 2310 miRNAs were finally predicted to have regulatory relationships with 51 DERATGs. The regulatory relationships were analyzed by network visualization (Fig. 8B). Finally, RBP genes were extracted from the RBPDB database. Correlation analysis was conducted to observe the correlation between RBP genes and 54 DERATGs in the two datasets (GSE55235 and GSE55457) separately, and the results were displayed as heat maps (Fig. 8C, D).

#### Construction of interaction networks between drugs and DERATGs targets

By retrieving the interaction relationship between DERATGs and drugs from the PharmGKB database, finally, we screened these drugs, adalimumab, hydroxyurea, platinum compounds, and so on from the 13 genes analyzed, *PTPRC*, *KLF4*, *HLA-DOB*, *EGFR*, *SOCS3*, *CXCL10*, *CCR5*, *MMP1*, *CXCL13*, *FKBP5*, *TYMS*, *IL7R*, and *MS4A1* (Fig. 9A). Additionally, we looked at the interaction network between DERATGs and targeted drugs through the DrugCentral database, screening for drugs such as ebastine, econazole, ibrutinib, necitumumab, etc., that are associated with *FKBP5*, *PSMB9*, *CCR5*, *MS4A1*, *CCR2*, *MMP1*, *TYMS*, *EGFR*, *CD2*, *JUN*, *CDS2*, *TNFRSF17*, *NR4A1*, and *LAP3* (Fig. 9B).

#### Immune infiltration analysis

The immune cell infiltration of the RA and the normal group samples in the GSE55235 and the GSE55457 datasets were analyzed based on the CIBERSORT algorithm. The immune infiltration of GSE55235 was analyzed, and a heat map was drawn (Fig. 10A). The unexpressed eosinophils cells were eliminated, and only the cells that were expressed in the sample, such as monocytes, follicular helper T cells, neutrophils, etc., were retained in the heat map. The image shows that plasma cells, naive B cells, etc., had a high infiltration level in the RA group, while resting dendritic cells, activated mast cells, etc.,

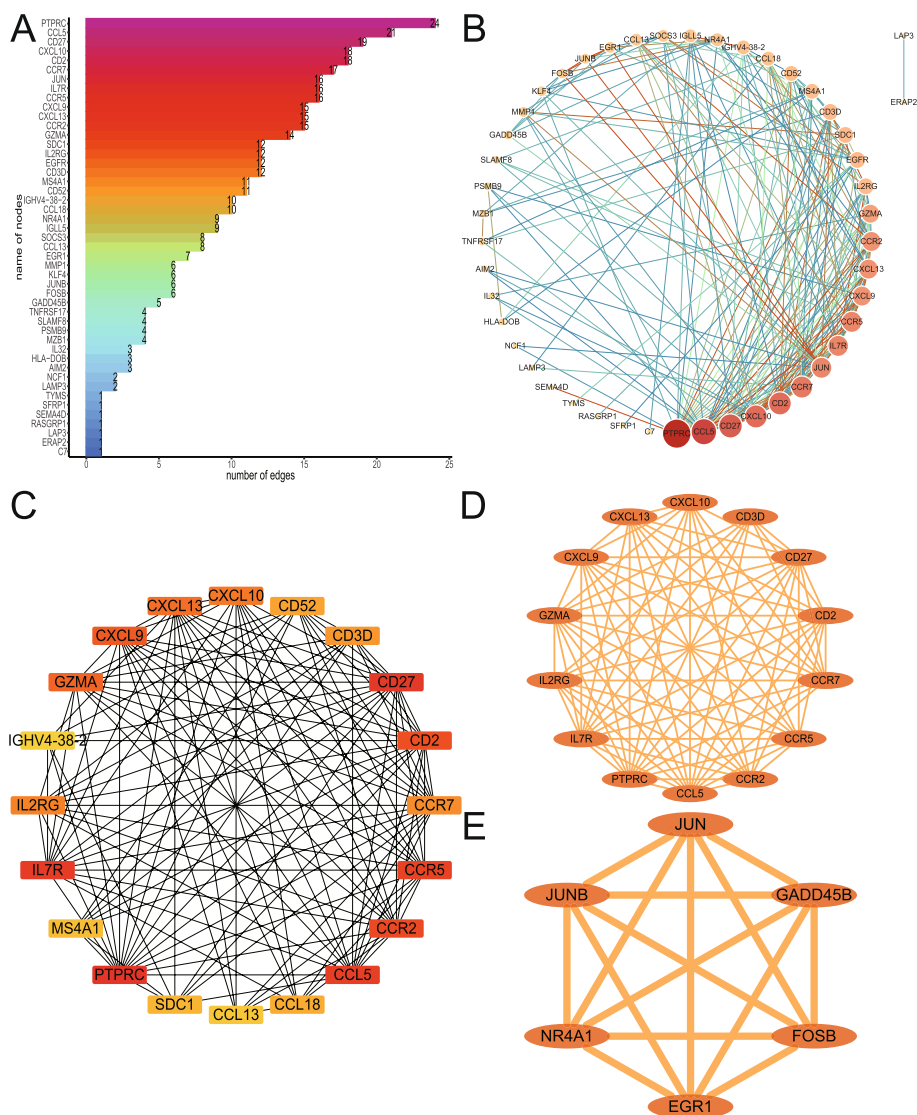


**Fig. 7** Protein–protein interaction network analysis of differentially expressed genes targeted by RA (DERATGs). **A** Data on the number of protein interaction relationships of DERATGs. **B** Protein interaction network of DERATGs. **C**. Network diagram of the top 20 hub nodes. **D, E** Protein interaction network subnetwork construction based on DERATGs, **D** Module 1 and **E** Module 2

had a low infiltration level. Immune cells from different groups were compared (Fig. 10B), and cells with significant differences ( $P < 0.05$ ) are displayed in the figure. Plasma cells, resting dendritic cells, gamma delta T cells, mast cells activated, and naive B cells differed significantly from the heat map. For the GSE55457 dataset, the immune infiltration heat map was also drawn (Fig. 10C). The unexpressed eosinophils cells were eliminated, and only the dendritic cells, monocytes were activated, neutrophils, etc., expressed in the sample were retained in the heat map. However, there was little infiltration of activated mast cells, dendritic cells, and so forth in the RA group. As shown in the figure, the RA group had high

levels of infiltration of plasma cells, naive B cells, and others. The differential comparison between groups of the GSE55457 dataset (Fig. 10D) revealed significant differences in the activation of M1 macrophages, plasma cells, naive B cells, follicular helper T cells, activated mast cells, and activated dendritic cells, which was consistent with the results of the GSE55235 dataset.

**Subtype construction based on immune infiltration analysis**

The immune cell infiltration of the RA and normal group samples in the GSE5235 and the GSE55457 datasets was analyzed using the ssGSEA algorithm. Finally, the

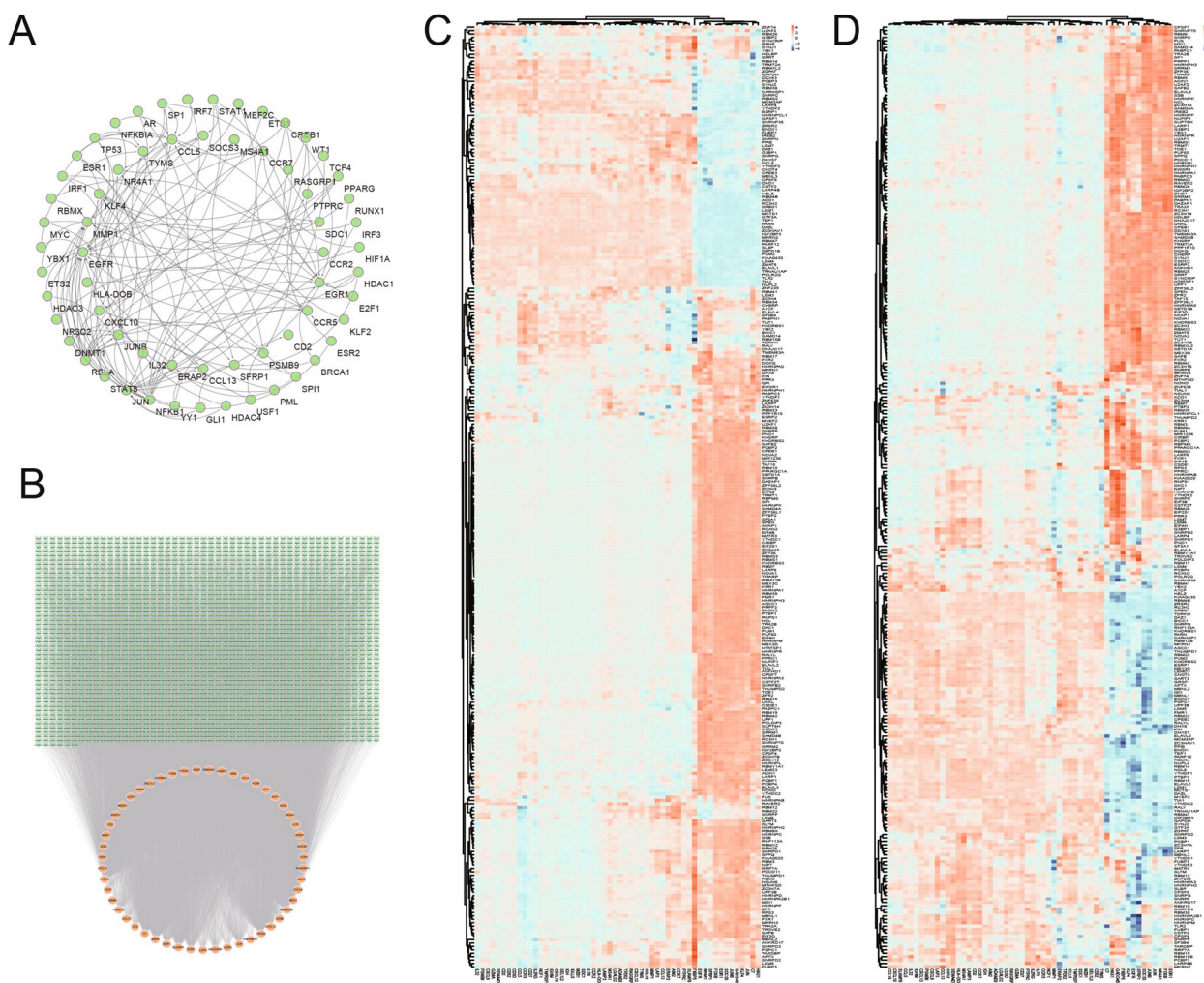


**Fig. 8** Construction of correlation network and RNA-binding protein (RBP) correlation analysis based on differentially expressed genes targeted by RA (DERATGs). **A** Transcription factor (TF)-target network for DERATGs. The arrow is directed toward the targeted DERATGs from the predicted TF. **B** Micro RNA (miRNA)-mRNA network. Red nodes represent DERATGs, green nodes represent related miRNAs, and lines represent the regulatory relationships between DERATGs and miRNAs. **C** Heat map of the correlation between 54 DERATGs and RBP genes in the expression profile of the GSE55235 dataset. Positively correlated genes are represented by red, whereas negatively correlated genes are represented by blue. **D** Heat map of the correlation between 54 DERATGs and RBP genes in the expression profile of the GSE55457 dataset. Positively correlated genes are represented by red, whereas negatively correlated genes are represented by blue

expression profiles of immune cells were obtained after the expression profiles were predicted and analyzed using 28 types of immune cell-specific marker genes. The RA samples were divided into two subtypes, Cluster1 and Cluster2, by high and low expression clustering (Fig. 11A, B). MDSC, eosinophil, activated CD4+ T cell, and other immune cells were highly expressed in Cluster1 but lowly expressed in Cluster2.

**Differential analysis of DERATGs between subtypes**

The expression of 54 DERATGs in various subtypes was analyzed following the RA subtypes in the GSE55235 and the GSE55457 datasets (Fig. 12A, B). The figure

shows the DERATGs that differ significantly ( $P < 0.05$ ). The *C7* gene was significantly expressed in Cluster2 of the GSE55235 dataset, while other significantly different DERATGs were strongly expressed in Cluster1 of the subtype. The *ERAP2* gene was highly expressed in Cluster2 of the GSE55457 dataset, whereas other significantly differential DERATGs were highly expressed in the Cluster1 subtype.

**Discussion**

To understand a universal marker assessment is our goal. However, the data sets utilized in this study did not precisely specify factors related to drugs,



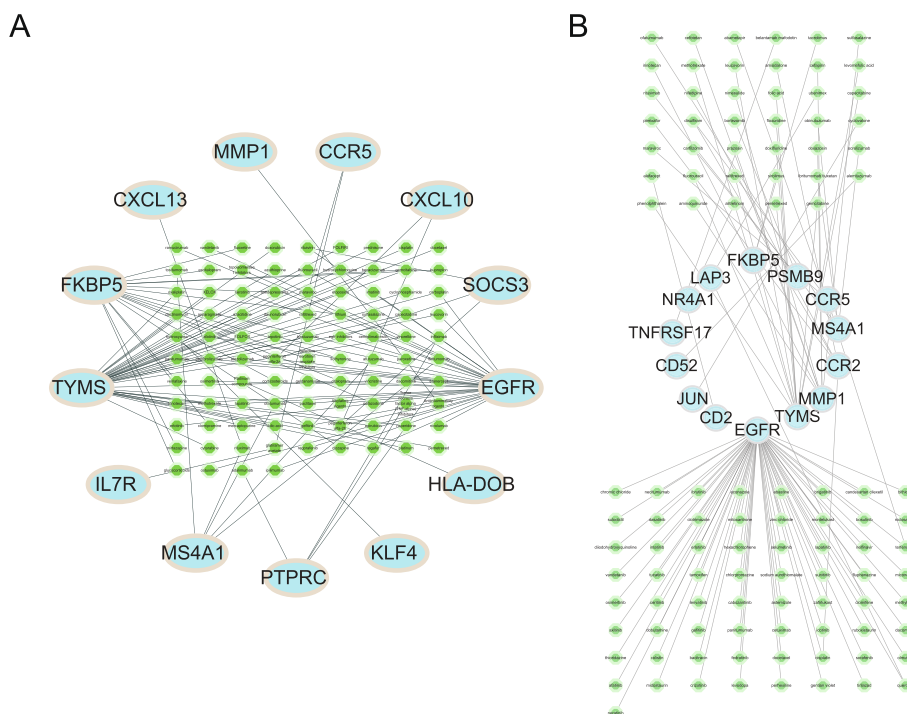


**Fig. 9** Construction of interaction networks between drugs and DERATGs targets. **A** The construction of a target-drug network via the PharmGKB database. **B** Construction of the target-drug network through the DrugCentral database. Blue indicates DERATGs, and green indicates the drugs predicted by DERATGs

vaccinations, age, environments, psychology, region, genetics or epidemiology. This does not imply that factors related to these factors did not affect the patients in these two data sets. We removed a few data sets with particular descriptions to prevent bias in this investigation to prevent the proportion of particular subjects from rising.

A total of 54 DERATGs were found by comparing the genes expressed in samples from patients with RA and normal groups. These DERATGs were strongly associated with inflammation and immune response. Although the absence of the well-known three RA star molecules TNF, IL6, and JAK in the DERATGs examined in this study, the KEGG enrichment data showed that DERATGs were enriched in the TNF signaling pathway. In studying biologically targeted drug therapy, these three molecules are often accompanied by biological processes or signaling pathways rather than being studied individually [28–30]. In other words, investigating what seems to be a single molecule is investigating the entire signaling pathway, but these star molecules play an undeniably crucial role in the signaling pathway. Moreover, we discovered several key molecules did not exhibit significant differences in expression changes in actual studies (such as GSEA and GSVA pathway analyses in this study). Therefore, the high setting of the gene screening

threshold may be why star molecules were absent from this study.

We performed GSVA and GSEA analyses by analyzing all gene expression data to evaluate further RA's complex signature of immune/inflammatory responses. Interestingly, the “Intestinal immune network for IgA production” showed high expression in our study, likely supporting our findings on the GMrepo online database. It has been noted that patients with RA (both new-onset and chronic) either showed IgA-like antibody responses to *Prevotella copri* (*P. copri*) or its 27-kDa protein, which are associated with the production of TH17 cell cytokines and the presence of ACPAs [31]. Additionally, intestinal tissue samples from patients with RA contain higher IgA antibodies that identify dietary antigens [32]. Presently, most RA microbiome studies focus on associations, which aim to link changes in the bacterial composition of the gastrointestinal tract with the condition. Although these findings suggest practical applicability, the mechanism by which gut flora influences the development of RA is still not fully understood [31]. Hence, our study may offer the opportunity to adapt more details and references for future research, diagnostics, and therapeutic approaches.

The inflammatory process in RA depends on chemokines. Multivariate discriminant analysis revealed

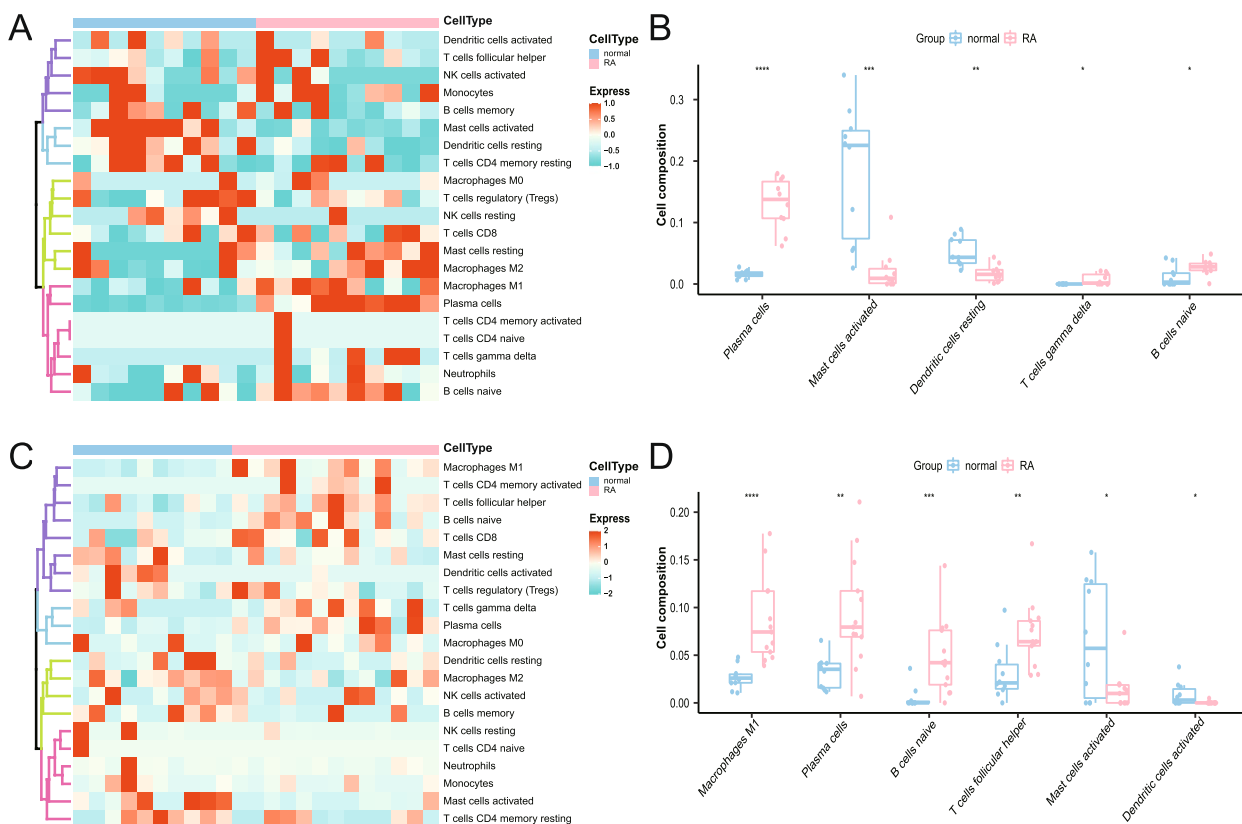


**Fig. 10** Investigation and visual representation of immune cell infiltration. **A** Heat map of immune infiltration in the GSE55235 dataset shows that rheumatoid arthritis (RA) is indicated by red cells and normal by blue cells. **B** A boxplot depicting significant differential immune infiltration cells in the GSE55235 dataset is colored red for the RA group and blue for the normal group. **C**. Heat map of immune infiltration in the GSE55457 dataset; red cells indicate RA and blue cells indicate normal. **D** A boxplot of the significant differentially immune infiltrating cells of the GSE55457 dataset is shown, with red for the RA group and blue for the normal group. \*\*\*\* $p < 0.0001$ , \*\*\* $p < 0.001$ , \*\* $p < 0.01$ , and \* $p < 0.05$

that chemokines *CXCL10* and *CXCL13* were significantly abundant in the blood plasma of patients with RA compared to healthy volunteers [33]. According to an in vitro study, abatacept's (ABT) most likely target molecule in inflamed rheumatoid joints is *CXCL10*, and serum *CXCL10* levels may be a feasible predictor of the therapeutic response to ABT treatment [34]. Previous studies have shown that *CCR5* DNA variation impacts the degree of RA severity [35] and that *CCR5* increases the chemotactic response in the synovial fluid of patients with RA [36]. A recent literature review reported that, undoubtedly, *CCR5* had gained its place in RA pathogenesis as an important genetic risk factor [37]. *PTPRC*, also known as *CD45* in some instances, performs several crucial regulatory functions that regulate cell growth, differentiation, mitosis, and malignant transformation [38]. It has been demonstrated to regulate T- and B-cell antigen receptor signaling [39]. In our study, the *PTPRC* gene plays a vital role in this signal transduction network. The *PTPRC* gene's roles in RA's pathogenesis are currently poorly understood.

However, four anti-TNF treatments—TNF- $\alpha$  inhibitors, adalimumab, infliximab, and etanercept—were linked to *PTPRC* in the drug-gene interaction network, demonstrating that *PTPRC* is a druggable gene that can be targeted by TNF- $\alpha$  inhibitors, adalimumab, infliximab, and etanercept. Additionally, *PTPRC* has been demonstrated to be the genetic biomarker of TNFi response most frequently replicated and useful for targeted therapy in patients with RA [40]. Unfortunately, neither IL-6 nor JAK inhibitors showed any evidence of a genetic relationship in our study. This supports the idea that biological processes, rather than specific molecules, are currently the focus of drug research. However, the druggable targets selected for this study offer a broad reference point for future research into new targets for old medicines.

In diseases like cancer, autoimmune disease, diabetes, and cardiovascular disease, TFs play a crucial biological role [41]. Although most TFs have traditionally been regarded as “undruggable” targets [41], current research has revealed that the tumor therapy drug Binimetinib may have a potential targeted binding impact with

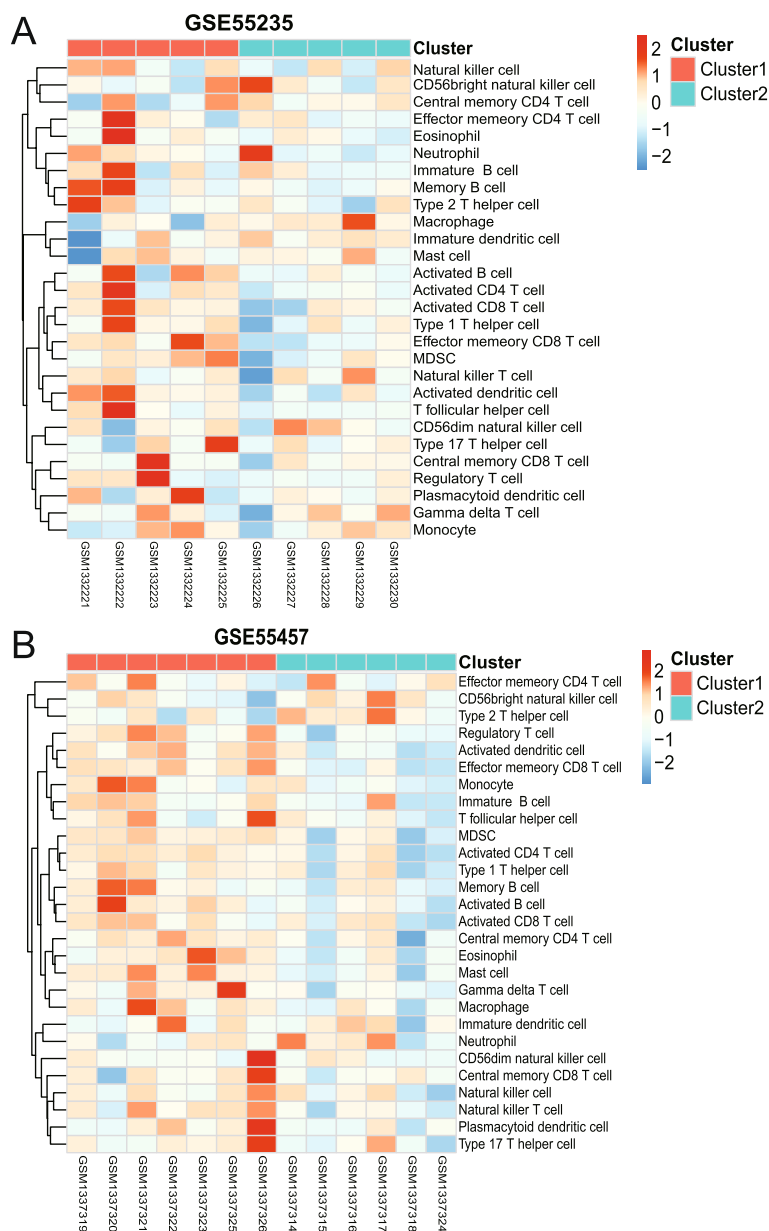


**Fig. 11** Rheumatoid arthritis sample subtype analysis. **A** Heat map of the 28 distinct types of immune cell infiltration in the GSE55235 dataset. Red and green symbolize the groups in Clusters 1 and 2, respectively. **B** Heat map of immune cell infiltration of 28 different kinds in the GSE55457 dataset. Red and green symbolize the groups in Clusters 1 and 2, respectively

NFKB1 [42]. Additionally, it has been reported that small molecule inhibitors can specifically target AR, making it the primary treatment target for advanced cancer [43]. This is also something that research has found. Combining ketoprofen and indolamide inhibits the Gli1-mediated transcription in the Hedgehog pathway [44]. It has been demonstrated that the novel oral active molecular gel WBC100 selectively degrades the protein c-Myc over

other proteins and effectively kills cancer cells that overexpress c-Myc [45]. Human triple-negative breast and gastric cancer xenografts have been demonstrated to regress in response to WZ-2-033, a new STAT3 inhibitor [46]. According to a study, a bromine domain and extra terminal domain inhibitor can induce tumor cell apoptosis by disrupting the specific transcription network that the TCF4 TF regulates [47]. However, other TFs in this

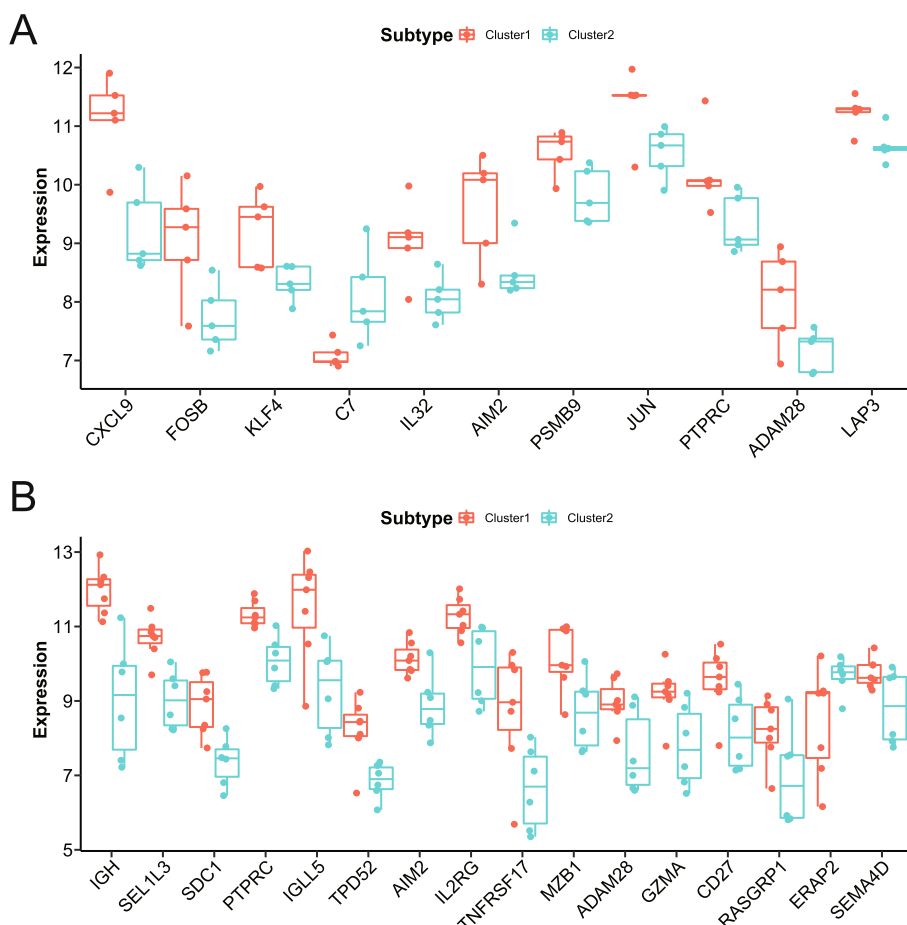


**Fig. 12** Differential analysis of DERATGs between subtypes. **A** The GSE55235 dataset expresses 11 DERATGs in two subtypes. Red and green symbolize the groups in Clusters 1 and 2, respectively. **B** The GSE55457 dataset expresses 16 DERATGs in two subtypes. Red and green symbolize the groups in Clusters 1 and 2, respectively

study have not consistently been reported to be pharmacologically actionable. In conclusion, although the majority of present work on druggable TFs focuses on cancer drug development, it also offers suggestions for work on RA-related druggable TFs. We believe that NFKB1, AR, GLI1, Myc, STAT3, and TCF4 are now the most potentially druggable TFs based on the regulatory relationship between TFs and DERATGs in this study.

Currently, cell-type deconvolution analysis is frequently applied in RA research. *FAS*, *MAPK8*, and *TNFSF10* may be associated with alterations in the immune microenvironment in patients with RA, according to a study that used CIBERSORT analysis [48]. It was discovered that *SLC2A3* is positively associated with the expression of activated mast cells in RA synovial tissue using immune cell infiltration [49]. The CIBERSORT study found that the RA key genes *CXCL8*, *CXCL2*, and *FADD* were associated with mast cells, monocytes, activated natural killer

cells, CD8 T cells, dormant dendritic cells, and plasma cells [50]. In this study, we performed a thorough analysis of the immune infiltration landscape using ssGSEA and CIBERSORT algorithms to quantify the profile of immune infiltration in RA. Studies have shown that 20% of the antibodies mature naive B cells produce when they reach the periphery are still autoreactive. This percentage is significantly higher in patients with RA [51, 52]. Rituximab, a therapeutic antibody that targets CD20, has been successfully used as a B cell therapy to treat RA. Over the last decade, additional RA studies have suggested that (autoreactive) B cells may contribute to the progression of the disease [53]. There has been no research on RA therapy targeting plasma cells, and the function of plasma cells in RA is still unknown [54].

Regarding the involvement of mast cells and dendritic cells (DC cells) in the pathogenesis of RA, conflicting results have also been found. Although most research

has focused on the role of mast cells in the pathogenesis of RA [55–60] and that immature and activated DC cell populations are present in the synovium of the inflamed joint [61]. We found that patients with RA had decreased mast cell and DC cell infiltration in their tissues. However, other studies have suggested that steroid use may be related to decreased mast cells and DC cells in patients with RA [62–64]. The specific cause of the decline in mast cells and DC cells in RA must be further investigated because it is unknown if the patients in this study were using corticosteroids or other drugs.

Cluster1 and Cluster2, subtypes of expression profiles, were identified based on immune cell expression. The purpose of the analysis was to provide a better understanding of the function and regulatory mechanisms of the immune system. We can better understand the function and regulatory mechanisms of immune cells by understanding the expression forms of each subtype through the analysis of gene expression in subtypes. Determine which subtypes share the most common characteristics to determine the most effective course of action. Additionally, subtype expression profiles can also aid in the discovery of novel therapeutic targets. We might identify potential genes or molecules to be used as therapeutic targets by analyzing the genes expressed in specific subtypes. However, further experimental verification is required. The findings indicate that the *PTPRC* gene was highly expressed in Cluster1 in the GSE55235 and GSE55457 datasets. *PTPRC* may be the characteristic gene of the Cluster1 subtype in these two datasets or play a significant biological function that may be directly associated with the function of this subtype. We also noticed discrepancies in the analysis results between the two data sets, which we believe may be due to a batch effect brought on by the differences in data set sample collection location, time and computer sequencing time. Another major limitation of this study is the batch effect.

This study has some other drawbacks. First, the study lacked clinically important details about the condition, such as disease activity and treatment usage. Additionally, no multi-group trials were conducted, and the study's sole focus was on the gene transcriptome. Finally, bioinformatics approaches limited data analysis; preclinical and clinical validation is required.

In conclusion, the scientific community needs to investigate and comprehend how gut microbiota, genetics, and immune inflammation are related to the etiology of RA. The findings of this study might be used as a reference for clinical diagnosis, prognosis, and targeted molecular treatment for RA.

## Appendix

**Table 7** Gene symbol

Gene.Symbol	Official.Full.Name
IGHM	immunoglobulin heavy constant mu
IGLL5	immunoglobulin lambda like polypeptide 5
MZB1	marginal zone B and B1 cell specific protein
SEL1L3	SEL1L family member 3
IGH	immunoglobulin heavy locus
CCR2	C–C motif chemokine receptor 2
NCF1	neutrophil cytosolic factor 1
SEMA4D	semaphorin 4D
SDC1	syndecan 1
CD2	CD2 molecule
CD52	CD52 molecule
PSMB9	proteasome 20S subunit beta 9
TYMS	thymidylate synthetase
CD3D	CD3 delta subunit of T-cell receptor complex
IL7R	interleukin 7 receptor
PTPRC	protein tyrosine phosphatase receptor type C
GZMA	granzyme A
RASGRP1	RAS guanyl releasing protein 1
CD27	CD27 molecule
CXCL13	C-X-C motif chemokine ligand 13
TNFRSF17	TNF receptor superfamily member 17
CCL5	C–C motif chemokine ligand 5
CCR5	C–C motif chemokine receptor 5
CXCL10	C-X-C motif chemokine ligand 10
CCL18	C–C motif chemokine ligand 18
IL2RG	interleukin 2 receptor subunit gamma
SLAMF8	SLAM family member 8
HLA-DOB	major histocompatibility complex, class II, DO beta
MMP1	matrix metalloproteinase 1
LAP3	leucine aminopeptidase 3
ADAM28	ADAM metalloproteinase domain 28
TPD52	tumor protein D52
IL32	interleukin 32
CXCL9	C-X-C motif chemokine ligand 9
AIM2	absent in melanoma 2
LAMP3	lysosomal associated membrane protein 3
LGALS2	galectin 2
CCR7	C–C motif chemokine receptor 7



Gene.Symbol	Official.Full.Name
CCL13	C–C motif chemokine ligand 13
MS4A1	membrane spanning 4-domains A1
ERAP2	endoplasmic reticulum aminopeptidase 2
KLF4	KLF transcription factor 4
GADD45B	growth arrest and DNA damage inducible beta
FOSB	FosB proto-oncogene, AP-1 transcription factor subunit
EGFR	epidermal growth factor receptor
SOCS3	suppressor of cytokine signaling 3
EGR1	early growth response 1
JUNB	JunB proto-oncogene, AP-1 transcription factor subunit
C7	complement C7
NR4A1	nuclear receptor subfamily 4 group A member 1
JUN	Jun proto-oncogene, AP-1 transcription factor subunit
HAS1	hyaluronan synthase 1
SFRP1	secreted frizzled related protein 1
FKBP5	FKBP prolyl isomerase 5
TNF	tumor necrosis factor
IL6	interleukin 6
JAK1	Janus kinase 1
JAK2	Janus kinase 2
JAK3	Janus kinase 3
TYK2	tyrosine kinase 2
NFKB1	nuclear factor kappa B subunit 1
AR	androgen receptor
GLI1	GLI family zinc finger 1
MYC	MYC proto-oncogene, bHLH transcription factor
STAT3	signal transducer and activator of transcription 3
TCF4	transcription factor 4
FAS	Fas cell surface death receptor
MAPK8	mitogen-activated protein kinase 8
TNFSF10	TNF superfamily member 10
SLC2A3	solute carrier family 2 member 3
CXCL8	C-X-C motif chemokine ligand 8
CXCL2	C-X-C motif chemokine ligand 2
FADD	Fas associated via death domain

## Supplementary Information

The online version contains supplementary material available at <https://doi.org/10.1186/s41065-024-00310-6>.

Additional file 1.

## Acknowledgements

We are grateful to the investigators who provided the publicly available microarray datasets.

## Authors' contributions

Professor Yue Wang designed this research. Yin Guan analyzed the data and wrote the manuscript. Yue Zhang searched for datasets and backgrounds. Xiaoqian Zhao revised the manuscript. All authors have read and agree to the published version of the manuscript. The author(s) read and approved the final manuscript.

## Funding

This work was supported by the National Natural Science Foundation of China (Grant numbers 81973769) and Postgraduate Research & Practice Innovation Program of Jiangsu Province (Grant numbers KYCX22\_1941).

## Availability of data and materials

The datasets GSE55235 and GSE55457 for this study can be found in the Gene Expression Omnibus database [<https://www.ncbi.nlm.nih.gov/geo/query/acc.cgi?acc=GSE55235/GSE55457>]; All the R code and supporting data for this article are available on the GitHub page created by the first author [<https://github.com/DrGuanYin686993/The-doctor-is-fond-of-milk.git>].

## Declarations

### Ethics approval and consent to participate

There is no ethics involved in.

### Consent for publication

Not acceptable.

### Competing interests

There is no competing interests.

### Author details

<sup>1</sup>Affiliated Hospital of Nanjing University of Chinese Medicine, Nanjing 210029, Jiangsu, China. <sup>2</sup>Department of Ethics Committee, Affiliated Hospital of Nanjing University of Chinese Medicine, Nanjing 210029, Jiangsu, China. <sup>3</sup>Department of Rheumatism Immunity Branch, Affiliated Hospital of Nanjing University of Chinese Medicine, No. 155 Hanzhong Road, Nanjing 210029, Jiangsu, China.

Received: 12 April 2023 Accepted: 12 January 2024

Published online: 25 January 2024

## References

- Conforti A, Di Cola I, Pavlych V, et al. Beyond the joints, the extra-articular manifestations in rheumatoid arthritis. *Autoimmun Rev.* 2021;20(2):102735. <https://doi.org/10.1016/j.autrev.2020.102735>. PMID:33346115.
- Chaurasia N, Singh A, Singh IL, et al. Cognitive dysfunction in patients of rheumatoid arthritis. *J Family Med Prim Care.* 2020;9(5):2219–25. [https://doi.org/10.4103/jfmpc.jfmpc\\_307\\_20](https://doi.org/10.4103/jfmpc.jfmpc_307_20). PMID:32754477.
- Lanes SF, Lanza LL, Radensky PW, et al. Resource utilization and cost of care for rheumatoid arthritis and osteoarthritis in a managed care setting: the importance of drug and surgery costs. *Arthritis Rheum.* 1997;40(8):1475–81. <https://doi.org/10.1002/art.1780400816>. PMID:9259428.
- Cooper NJ. Economic burden of rheumatoid arthritis: a systematic review. *Rheumatology (Oxford).* 2000;39(1):28–33. <https://doi.org/10.1093/rheumatology/39.1.28>. PMID:10662870.
- Coffey CM, Crowson CS, Myasoedova E, et al. Evidence of diagnostic and treatment delay in seronegative rheumatoid arthritis: missing the window of opportunity. *Mayo Clin Proc.* 2019;94(11):2241–8. <https://doi.org/10.1016/j.mayocp.2019.05.023>. PMID:31619364.

6. Banal F, Dougados M, Combescuré C, et al. Sensitivity and specificity of the American College of Rheumatology 1987 criteria for the diagnosis of rheumatoid arthritis according to disease duration: a systematic literature review and meta-analysis. *Ann Rheum Dis*. 2009;68(7):1184–91. <https://doi.org/10.1136/ard.2008.093187>. PMID:18728049.
7. Smolen JS, Aletaha D, McInnes IB. Rheumatoid arthritis. *Lancet*. 2016;388(10055):2023–38. [https://doi.org/10.1016/s0140-6736\(16\)30173-8](https://doi.org/10.1016/s0140-6736(16)30173-8). PMID:27156434.
8. Dai D, Zhu J, Sun C, et al. GMrepo v2: a curated human gut microbiome database with special focus on disease markers and cross-dataset comparison. *Nucleic Acids Res*. 2022;50(D1):D777–d784. <https://doi.org/10.1093/nar/gkab1019>. PMID:34788838.
9. Woetzel D, Huber R, Kupfer P, et al. Identification of rheumatoid arthritis and osteoarthritis patients by transcriptome-based rule set generation. *Arthritis Res Ther*. 2014;16(2):R84. <https://doi.org/10.1186/ar4526>. PMID:24690414.
10. Davis S, Meltzer PS. GEOquery: a bridge between the Gene Expression Omnibus (GEO) and BioConductor. *Bioinformatics*. 2007;23(14):1846–7. <https://doi.org/10.1093/bioinformatics/btm254>. PMID:17496320.
11. Gautier L, Cope L, Bolstad BM, et al. affy—analysis of Affymetrix GeneChip data at the probe level. *Bioinformatics*. 2004;20(3):307–15. <https://doi.org/10.1093/bioinformatics/btg405>. PMID:14960456.
12. C.-I. L. Developer S, Guo Y, Sheng Q, Shyr Y. RnaSeqSampleSize: RnaSeqSampleSize\_R package version 2.5.1. 2021.
13. Ritchie ME, Phipps B, Wu D, et al. Limma powers differential expression analyses for RNA-seq and microarray studies. *Nucleic Acids Res*. 2015;43(7):e47. <https://doi.org/10.1093/nar/gkv007>. PMID:25605792.
14. Safran M, Dalah I, Alexander J, et al. GeneCards version 3: the human gene integrator. *Database (Oxford)*. 2010;2010:baq020. <https://doi.org/10.1093/database/baq020>. PMID:20689021.
15. Yu G, Wang LG, Han Y, et al. clusterProfiler: an R package for comparing biological themes among gene clusters. *OMICS*. 2012;16(5):284–7. <https://doi.org/10.1089/omi.2011.0118>. PMID:22455463.
16. Yu G, Wang LG, Yan GR, et al. DOSE: an R/Bioconductor package for disease ontology semantic and enrichment analysis. *Bioinformatics*. 2015;31(4):608–9. <https://doi.org/10.1093/bioinformatics/btu684>. PMID:25677125.
17. Hänzelmann S, Castelo R, Guinney J. GSEA: gene set variation analysis for microarray and RNA-seq data. *BMC Bioinformatics*. 2013;14:7. <https://doi.org/10.1186/1471-2105-14-7>. PMID:23323831.
18. Szklarczyk D, Gable AL, Lyon D, et al. STRING v11: protein-protein association networks with increased coverage, supporting functional discovery in genome-wide experimental datasets. *Nucleic Acids Res*. 2019;47(D1):D607–d613. <https://doi.org/10.1093/nar/gky1131>. PMID:30476243.
19. Shannon P, Markiel A, Ozier O, et al. Cytoscape: a software environment for integrated models of biomolecular interaction networks. *Genome Res*. 2003;13(11):2498–504. <https://doi.org/10.1101/gr.1239303>. PMID:14597658.
20. Bader GD, Hogue CW. An automated method for finding molecular complexes in large protein interaction networks. *BMC Bioinformatics*. 2003;4:2. <https://doi.org/10.1186/1471-2105-4-2>. PMID:12525261.
21. Han H, Cho JW, Lee S, et al. TRRUST v2: an expanded reference database of human and mouse transcriptional regulatory interactions. *Nucleic Acids Res*. 2018;46(D1):D380–d386. <https://doi.org/10.1093/nar/gkx1013>. PMID:29087512.
22. Gong L, Whirl-Carrillo M, Klein TE. PharmGKB, an Integrated resource of pharmacogenomic knowledge. *Curr Protoc*. 2021;1(8):e226. <https://doi.org/10.1002/cpz1.226>. PMID:34387941.
23. Avram S, Wilson TB, Curpan R, et al. DrugCentral 2023 extends human clinical data and integrates veterinary drugs. *Nucleic Acids Res*. 2023;51(D1):D1276–d1287. <https://doi.org/10.1093/nar/gkac1085>. PMID:36484092.
24. Shin C, Nam JW, Farh KK, et al. Expanding the microRNA targeting code: functional sites with centered pairing. *Mol Cell*. 2010;38(6):789–802. <https://doi.org/10.1016/j.molcel.2010.06.005>. PMID:20620952.
25. Cook KB, Kazan H, Zuberi K, et al. RBPDB: a database of RNA-binding specificities. *Nucleic Acids Res*. 2011;39(Database issue):D301–8. <https://doi.org/10.1093/nar/gkq1069>. PMID:21036867.
26. Newman AM, Liu CL, Green MR, et al. Robust enumeration of cell subsets from tissue expression profiles. *Nat Methods*. 2015;12(5):453–7. <https://doi.org/10.1038/nmeth.3337>. PMID:25822800.
27. Ye L, Zhang T, Kang Z, et al. Tumor-infiltrating immune cells act as a marker for prognosis in colorectal cancer. *Front Immunol*. 2019;10:2368. <https://doi.org/10.3389/fimmu.2019.02368>. PMID:31681276.
28. Wu J, Feng Z, Chen L, et al. TNF antagonist sensitizes synovial fibroblasts to ferroptotic cell death in collagen-induced arthritis mouse models. *Nat Commun*. 2022;13(1):676. <https://doi.org/10.1038/s41467-021-27948-4>. PMID:35115492.
29. Baldini C, Moriconi FR, Galimberti S, et al. The JAK-STAT pathway: an emerging target for cardiovascular disease in rheumatoid arthritis and myeloproliferative neoplasms. *Eur Heart J*. 2021;42(42):4389–400. <https://doi.org/10.1093/eurheartj/ehab447>. PMID:34343257.
30. Takeuchi T, Yoshida H, Tanaka S. Role of interleukin-6 in bone destruction and bone repair in rheumatoid arthritis. *Autoimmun Rev*. 2021;20(9):102884. <https://doi.org/10.1016/j.autrev.2021.102884>. PMID:34229044.
31. Zaiss MM, Joyce Wu HJ, Mauro D, et al. The gut-joint axis in rheumatoid arthritis. *Nat Rev Rheumatol*. 2021;17(4):224–37. <https://doi.org/10.1038/s41584-021-00585-3>. PMID:33674813.
32. Hvatum M, Kanerud L, Hällgren R, et al. The gut-joint axis: cross reactive food antibodies in rheumatoid arthritis. *Gut*. 2006;55(9):1240–7. <https://doi.org/10.1136/gut.2005.076901>. PMID:16484508.
33. Pandya JM, Lundell AC, Andersson K, et al. Blood chemokine profile in untreated early rheumatoid arthritis: CXCL10 as a disease activity marker. *Arthritis Res Ther*. 2017;19(1):20. <https://doi.org/10.1186/s13075-017-1224-1>. PMID:28148302.
34. Yukawa K, Mokuda S, Kohno H, et al. Serum CXCL10 levels are associated with better responses to abatacept treatment of rheumatoid arthritis. *Clin Exp Rheumatol*. 2020;38(5):956–963. <https://doi.org/10.1007/s10067-020-01969-2>. PMID:32422904.
35. Zapico I, Coto E, Rodríguez A, et al. CCR5 (chemokine receptor-5) DNA polymorphism influences the severity of rheumatoid arthritis. *Genes Immun*. 2000;1(4):288–9. <https://doi.org/10.1038/sj.gene.6363673>. PMID:11196706.
36. Koch AE, Kunkel SL, Harlow LA, et al. Macrophage inflammatory protein-1 alpha. A novel chemotactic cytokine for macrophages in rheumatoid arthritis. *J Clin Invest*. 1994;93(3):921–8. <https://doi.org/10.1172/jci117097>. PMID:8132778.
37. Aletaha D, Smolen JS. Diagnosis and management of rheumatoid arthritis: a review. *JAMA*. 2018;320(13):1360–72. <https://doi.org/10.1001/jama.2018.13103>. PMID:30285183.
38. Rheinländer A, Schraven B, Bommhardt U. CD45 in human physiology and clinical medicine. *Immunol Lett*. 2018;196:22–32. <https://doi.org/10.1016/j.imlet.2018.01.009>. PMID:29366662.
39. Hendriks WJ, Pulido R. Protein tyrosine phosphatase variants in human hereditary disorders and disease susceptibilities. *Biochim Biophys Acta*. 2013;1832(10):1673–96. <https://doi.org/10.1016/j.bbadis.2013.05.022>. PMID:23707412.
40. Ferreira-Iglesias A, Montes A, Perez-Pampin E, et al. Replication of PTPRC as genetic biomarker of response to TNF inhibitors in patients with rheumatoid arthritis. *Pharmacogenomics J*. 2016;16(2):137–40. <https://doi.org/10.1038/tpj.2015.29>. PMID:25896535.
41. Lambert SA, Jolma A, Campitelli LF, et al. The human transcription factors. *Cell*. 2018;172(4):650–65. <https://doi.org/10.1016/j.cell.2018.01.029>. PMID:29425488.
42. Zheng X, Zheng Y, Wang J, et al. Binimetinib ameliorates the severity of septic cardiomyopathy by downregulating inflammatory factors. *Int Immunopharmacol*. 2022;113(Pt B):109454. <https://doi.org/10.1016/j.intimp.2022.109454>. PMID:36427477.
43. Kaikkonen S, Paakinaho V, Sutinen P, et al. Prostaglandin 15d-PGJ(2) inhibits androgen receptor signaling in prostate cancer cells. *Mol Endocrinol*. 2013;27(2):212–23. <https://doi.org/10.1210/me.2012-1313>. PMID:23192983.
44. Mahindroo N, Connelly MC, PUNCHIHEWA C, et al. Amide conjugates of ketoprofen and indole as inhibitors of Gli1-mediated transcription in the Hedgehog pathway. *Bioorg Med Chem*. 2010;18(13):4801–11. <https://doi.org/10.1016/j.bmc.2010.05.001>. PMID:20605720.
45. Xu Y, Yu Q, Wang P, et al. A selective small-molecule c-Myc degrader potently regresses lethal c-Myc overexpressing tumors. *Adv Sci (Weinh)*. 2022;9(8):e2104344. <https://doi.org/10.1002/adv.202104344>. PMID:35048559.
46. Zhong Y, Deng L, Shi S, et al. The novel STAT3 inhibitor WZ-2-033 causes regression of human triple-negative breast cancer and gastric cancer xenografts. *Acta Pharmacol Sin*. 2022;43(4):1013–23. <https://doi.org/10.1038/s41401-021-00718-0>. PMID:34267347.
47. Ceribelli M, Hou ZE, Kelly PN, et al. A druggable TCF4- and BRD4-dependent transcriptional network sustains malignancy in blastic plasmacytoid dendritic cell neoplasm. *Cancer Cell*. 2016;30(5):764–78. <https://doi.org/10.1016/j.ccell.2016.10.002>. PMID:27846392.

48. He Q, Ding H. Bioinformatics analysis of rheumatoid arthritis tissues identifies genes and potential drugs that are expressed specifically. *Sci Rep.* 2023;13(1):4508. <https://doi.org/10.1038/s41598-023-31438-6>. PMID:36934132.
49. Xiang J, Chen H, Lin Z, et al. Identification and experimental validation of ferroptosis-related gene SLC2A3 is involved in rheumatoid arthritis. *Eur J Pharmacol.* 2023;943:175568. <https://doi.org/10.1016/j.ejphar.2023.175568>. PMID:36736942.
50. Chen Y, Liao R, Yao Y, et al. Machine learning to identify immune-related biomarkers of rheumatoid arthritis based on WGCNA network. *Clin Rheumatol.* 2022;41(4):1057–68. <https://doi.org/10.1007/s10067-021-05960-9>. PMID:34767108.
51. Wardemann H, Yurasov S, Schaefer A, et al. Predominant autoantibody production by early human B cell precursors. *Science.* 2003;301(5638):1374–7. <https://doi.org/10.1126/science.1086907>. PMID:12920303.
52. Samuels J, Ng YS, Coupillaud C, et al. Impaired early B cell tolerance in patients with rheumatoid arthritis. *J Exp Med.* 2005;201(10):1659–67. <https://doi.org/10.1084/jem.20042321>. PMID:15897279.
53. Cambridge G, Leandro MJ, Edwards JC, et al. Serologic changes following B lymphocyte depletion therapy for rheumatoid arthritis. *Arthritis Rheum.* 2003;48(8):2146–54. <https://doi.org/10.1002/art.11181>. PMID:12905467.
54. Volkov M, van Schie KA, van der Woude D. Autoantibodies and B Cells: the ABC of rheumatoid arthritis pathophysiology. *Immunol Rev.* 2020;294(1):148–63. <https://doi.org/10.1111/immr.12829>. PMID:31845355.
55. Gotis-Graham I, McNeil HP. Mast cell responses in rheumatoid synovium. Association of the MCTC subset with matrix turnover and clinical progression. *Arthritis Rheum.* 1997;40(3):479–89. <https://doi.org/10.1002/art.1780400314>. PMID:9082936.
56. Triggiani M, Gentile M, Secondo A, et al. Histamine induces exocytosis and IL-6 production from human lung macrophages through interaction with H1 receptors. *J Immunol.* 2001;166(6):4083–91. <https://doi.org/10.4049/jimmunol.166.6.4083>. PMID:11238657.
57. Irie A, Takami M, Kubo H, et al. Heparin enhances osteoclastic bone resorption by inhibiting osteoprotegerin activity. *Bone.* 2007;41(2):165–74. <https://doi.org/10.1016/j.bone.2007.04.190>. PMID:17560185.
58. Kim KW, Kim BM, Lee KA, et al. Histamine and histamine H4 receptor promotes osteoclastogenesis in rheumatoid arthritis. *Sci Rep.* 2017;7(1):1197. <https://doi.org/10.1038/s41598-017-01101-y>. PMID:28446753.
59. van der Velden D, Lagraauw HM, Wezel A, et al. Mast cell depletion in the preclinical phase of collagen-induced arthritis reduces clinical outcome by lowering the inflammatory cytokine profile. *Arthritis Res Ther.* 2016;18(1):138. <https://doi.org/10.1186/s13075-016-1036-8>. PMID:27296719.
60. Kim KW, Kim BM, Won JY, et al. Regulation of osteoclastogenesis by mast cell in rheumatoid arthritis. *Arthritis Res Ther.* 2021;23(1):124. <https://doi.org/10.1186/s13075-021-02491-1>. PMID:33882986.
61. Page G, Lebecque S, Miossec P. Anatomic localization of immature and mature dendritic cells in an ectopic lymphoid organ: correlation with selective chemokine expression in rheumatoid synovium. *J Immunol.* 2002;168(10):5333–41. <https://doi.org/10.4049/jimmunol.168.10.5333>. PMID:11994492.
62. Schramm R, Thorlacius H. Neutrophil recruitment in mast cell-dependent inflammation: inhibitory mechanisms of glucocorticoids. *Inflamm Res.* 2004;53(12):644–52. <https://doi.org/10.1007/s00011-004-1307-8>. PMID:15654511.
63. Malone DG, Wilder RL, Saavedra-Delgado AM, et al. Mast cell numbers in rheumatoid synovial tissues. Correlations with quantitative measures of lymphocytic infiltration and modulation by antiinflammatory therapy. *Arthritis Rheum.* 1987;30(2):130–7. <https://doi.org/10.1002/art.1780300202>. PMID:3548731.
64. Yang H, Xia L, Chen J, et al. Stress-glucocorticoid-TSC22D3 axis compromises therapy-induced antitumor immunity. *Nat Med.* 2019;25(9):1428–41. <https://doi.org/10.1038/s41591-019-0566-4>. PMID:31501614.

## Publisher's Note

Springer Nature remains neutral with regard to jurisdictional claims in published maps and institutional affiliations.